Mutant α2-chimaerin signals via bidirectional ephrin pathways in Duane retraction syndrome

Alicia A. Nugent,[1,2,3] Jong G. Park,[1,2,4,5] Yan Wei,[1,2] Alan P. Tenney,[1,2,6] Nicole M. Gilette,[1,2] Michelle M. DeLisle,[1,2] Wai-Man Chan,[1,2,4,6] Long Cheng,[1,2,6] and Elizabeth C. Engle[1,2,3,4,6,7,8]

[1]Department of Neurology and [2]FM Kirby Neurobiology Center, Boston Children's Hospital, Boston, Massachusetts, USA. [3]Program in Neuroscience, Harvard Medical School, Boston, Massachusetts, USA. [4]Howard Hughes Medical Institute, Chevy Chase, Maryland, USA. [5]Duke University School of Medicine, Durham, North Carolina, USA. [6]Department of Neurology, Harvard Medical School, Boston, Massachusetts, USA. [7]Department of Ophthalmology, Boston Children's Hospital, Boston, Massachusetts, USA. [8]Department of Ophthalmology, Harvard Medical School, Boston, Massachusetts, USA.

Duane retraction syndrome (DRS) is the most common form of congenital paralytic strabismus in humans and can result from α2-chimaerin (*CHN1*) missense mutations. We report a knockin α2-chimaerin mouse (*Chn1*$^{KI/KI}$) that models DRS. Whole embryo imaging of *Chn1*$^{KI/KI}$ mice revealed stalled abducens nerve growth and selective trochlear and first cervical spinal nerve guidance abnormalities. Stalled abducens nerve bundles did not reach the orbit, resulting in secondary aberrant misinnervation of the lateral rectus muscle by the oculomotor nerve. By contrast, *Chn1*$^{KO/KO}$ mice did not have DRS, and embryos displayed abducens nerve wandering distinct from the *Chn1*$^{KI/KI}$ phenotype. Murine embryos lacking EPH receptor A4 (*Epha4*$^{KO/KO}$), which is upstream of α2-chimaerin in corticospinal neurons, exhibited similar abducens wandering that paralleled previously reported gait alterations in *Chn1*$^{KO/KO}$ and *Epha4*$^{KO/KO}$ adult mice. Findings from *Chn1*$^{KI/KI}$ *Epha4*$^{KO/KO}$ mice demonstrated that mutant α2-chimaerin and EphA4 have different genetic interactions in distinct motor neuron pools: abducens neurons use bidirectional ephrin signaling via mutant α2-chimaerin to direct growth, while cervical spinal neurons use only ephrin forward signaling, and trochlear neurons do not use ephrin signaling. These findings reveal a role for ephrin bidirectional signaling upstream of mutant α2-chimaerin in DRS, which may contribute to the selective vulnerability of abducens motor neurons in this disorder.

Introduction

Despite the complexity of axon guidance during neurodevelopment and its importance for proper circuit formation and normal behavior, few human disorders have been shown with certainty to result from abnormalities in this process. The precise alignment and coordinated movement of the eyes create a sensitive system to identify pathologic innervation of the extraocular muscles (EOMs) that arises during development (1, 2). Neurogenic forms of strabismus serve as models to investigate axon guidance mechanisms that are relevant to human development.

The ocular motor system comprises the oculomotor, trochlear, and abducens cranial nerves, which project to 7 EOMs (3) (Supplemental Figure 1A; supplemental material available online with this article; https://doi.org/10.1172/JCI88502DS1). Duane retraction syndrome (DRS) is a form of paralytic strabismus that results from altered ocular motor circuitry. Affected individuals cannot move one or both eyes laterally toward the ear (limited abduction), and upon attempted medial eye movement toward the nose (adduction), the globe(s) retract into the orbit. Autopsy, MRI, and electromyography studies of affected individuals have revealed loss of abducens motor neurons and nerve, which normally innervates the lateral rectus muscle to abduct the eye (4–6), and aberrant innervation of the lateral rectus by axons from the oculomotor nerve, which causes co-contraction of the medial and lateral recti on attempted adduction and retraction of the globe into the orbit (5–7) (Supplemental Figure 1B).

Genetic studies of pedigrees segregating DRS as an autosomal dominant trait identified gain-of-function missense mutations in *CHN1* that enhance the normal activity of the encoded protein α2-chimaerin (3, 8, 9). α2-Chimaerin–encoding mRNA is expressed in nearly all central and peripheral developing neurons in rodent embryos (10) and displays widespread neuronal expression at Carnegie stage 15/16 in developing human embryos, including rhombomere 5, where abducens neurons are located (3). Remarkably, despite broad neuronal expression of α2-chimaerin, the phenotype of affected individuals with *CHN1* mutations is limited to disordered eye movements. While clinical data and *CHN1* mutations support a neurogenic rather than myogenic etiology for DRS (3, 4, 9), the precise cellular and molecular mechanisms underlying its neurogenic etiology remain unknown.

α2-Chimaerin is a Rac GTPase-activating protein (RacGAP) reported to regulate cytoskeletal dynamics (11–15) and exists in an autoinhibited form until it is recruited to the plasma membrane and activated by upstream signaling (16, 17). Once activated, the α2-chimaerin GAP domain induces hydrolysis of Rac-GTP to inactive Rac-GDP, which alters actin dynamics and generates growth cone collapse (12–14, 16). Reported human *CHN1* mutations enhance RacGAP activity to further reduce Rac-GTP levels when overexpressed in heterologous cells (3, 9). α2-Chimaerin is reported to act downstream of several receptors implicated in axon growth and guidance, including EPH receptor A4 (EphA4), TrkB, and neu-

Conflict of interest: The authors have declared that no conflict of interest exists.
Submitted: May 11, 2016; **Accepted:** February 2, 2017.
Reference information: *J Clin Invest*. 2017;127(5):1664–1682.
https://doi.org/10.1172/JCI88502.

ropilin 1/plexinA (11–16, 18). *Epha4*$^{KO/KO}$ and *Chn1*$^{KO/KO}$ adult mice have a rabbit-like hopping gait, resulting from aberrant re-crossing of the corticospinal tract and miswiring of spinal interneurons that regulate central pattern generator (CPG) circuitry within the spinal cord (12, 14, 15, 19–22). α2-Chimaerin, furthermore, has been shown to interact with phosphorylated residues on EphA4 to alter cytoskeletal dynamics and elicit growth cone collapse (12, 13, 15).

Overexpression of DRS-mutant α2-chimaerin in the oculomotor nerve of chick and zebrafish was reported to cause oculomotor nerve stalling and/or branching defects (3, 18, 23). The primary DRS phenotype, however, was recently shown to arise from developmental absence of the abducens nerve and the subsequent ectopic innervation of its lateral rectus muscle target by the oculomotor nerve (24). These data suggest that *CHN1* mutations are more likely to cause primary defects in abducens rather than oculomotor nerve development. Thus, the developmental etiology and molecular mechanisms underlying DRS in the abducens and oculomotor nerves in the presence of endogenously hyperactive α2-chimaerin required further investigation.

Here, we establish a *Chn1* mutant knockin mouse model of DRS and find that *Chn1* mutations alter the primary development of the abducens, trochlear, and C1 nerves. Mechanistically, we find that these three different motor neuron populations harness ephrin/EphA4-mediated signaling pathways upstream of mutant α2-chimaerin in distinct manners to guide developing axons. Our data illustrate the neurodevelopmental pathology and etiology of DRS, provide insight into the selective vulnerability of the abducens nerve to gain-of-function α2-chimaerin mutations, and highlight the complexity of motor neuron guidance.

Results

α2-Chimaerin mutations in DRS are gain-of-function and alter abducens nerve development. To investigate the etiology of DRS, we generated a *Chn1*-knockin mouse model harboring an L20F amino acid substitution (*Chn1*$^{KI/KI}$), which is specific to the α2 isoform of chimaerin. This substitution segregated in a family with DRS and, following activation with PMA, enhanced α2-chimaerin membrane translocation, dimerization of WT and mutant α2-chimaerin, and RacGAP activity in vitro (3). We flanked exon 3 of the knockin construct with LoxP sites to permit generation of a conditional α2-chimaerin–knockout mouse upon exposure to Cre-recombinase (*Chn1*$^{KO/KO}$) (Supplemental Figure 1, C–E). *Chn1*$^{KI/KI}$ mice were born at the expected Mendelian frequency, were fertile, and had a normal lifespan.

In order to determine whether α2-chimaerin was constitutively active in neurons under endogenous expression of mutant protein, we cultured cortical neurons to assess Rac-GTP levels. We found that Rac-GTP levels did not differ between *Chn1*$^{WT/WT}$ and *Chn1*$^{KI/KI}$ cultured cortical neurons without stimulation, demonstrating that α2-chimaerin is not constitutively active in cortical neurons. However, upon addition of PMA to broadly activate α2-chimaerin irrespective of upstream pathway activation, mutant cultures had a marked reduction in Rac-GTP levels compared with WT cultures, demonstrating that the endogenous L20F amino acid substitution enhances GAP activity of α2-chimaerin upon activation (Supplemental Figure 1F), similar to previous overexpression experiments in non-neuronal cells (3, 9).

Chn1$^{WT/KI}$ and *Chn1*$^{KI/KI}$ mice exhibited unilateral or bilateral globe retraction of 61% and 72% penetrance that was not detected in *Chn1*$^{WT/WT}$ or *Chn1*$^{KO/KO}$ mice (Figure 1, A–C), confirming that human mutations are gain-of-function. Human DRS eye movement abnormalities were present from birth, and α2-chimaerin was expressed in oculomotor, trochlear, abducens, and spinal motor neurons by E11.5 (Supplemental Figure 2, A–D), as well as nearly all other neuronal types during embryonic and early postnatal development (3, 10). Humans carrying *CHN1*-DRS mutations are cognitively normal (25), and *Chn1*$^{KI/KI}$ mice displayed normal brain morphology (Supplemental Figure 2, E–H). Thus, we hypothesized that DRS-mutant α2-chimaerin selectively perturbs ocular motor system development. We crossed *Chn1*$^{KI/KI}$ and *Chn1*$^{KO/KO}$ mice to existing motor neuron and pancreas homeobox 1–GFP (*Hb9*-GFP) transgenic mice, as *Hb9* expression marks the abducens motor neurons but is absent from neighboring facial motor neurons (26), and used 3D visualization of whole mount E11.5 *Hb9*-GFP embryos stained with neurofilament to evaluate initial cranial nerve development (27) (Figure 1, D–F, and Supplemental Videos 1–3).

At E11.5, the *Chn1*$^{WT/WT}$ abducens nerve exited the hindbrain as multiple defasciculated nerve bundles (Figure 1G, area 1), which then fasciculated midway between the hindbrain and orbit (Figure 1G, area 2) before defasciculating again upon reaching the primitive EOM anlage at the orbit (Figure 1G, area 3, and Supplemental Video 1). Compared with *Chn1*$^{WT/WT}$, the *Chn1*$^{KI/KI}$ abducens nerve had fewer exiting bundles that appeared to be over-fasciculated in area 1 (Figure 1, H, and J) and stalled with variable penetrance in area 2 (Figure 1H, Supplemental Figure 2I, and Supplemental Video 2). Measurements of the abducens nerve from its hindbrain exit to the orbit indicated a 21% reduction in *Chn1*$^{WT/KI}$ embryos and 30% reduction in *Chn1*$^{KI/KI}$ embryos compared with WT (Figure 1K, $n = 5$ embryos per genotype). *Chn1*$^{WT/KI}$ and *Chn1*$^{KI/KI}$ embryos also displayed absence or thinning of the abducens nerve at area 3, reflected by a significant reduction in abducens nerve diameter near the orbit (Figure 1L and Supplemental Figure 2J).

By contrast, the *Chn1*$^{KO/KO}$ abducens nerve exited with an increased number of defasciculated bundles within area 1, some of which wandered dorsally toward the hindbrain or ventrally to track along the developing buccal branch of the facial nerve, also with variable penetrance (Figure 1, I and J). A subset of bundles in all *Chn1*$^{KO/KO}$ embryos, however, successfully fasciculated within area 2 and innervated the EOM anlage within area 3 (Figure 1I and Supplemental Video 3). While *Chn1*$^{KO/KO}$ abducens nerve length did not significantly differ from that in WT (Figure 1K), abducens nerve diameter was significantly greater (Figure 1L). Thus, the *Chn1*$^{KI/KI}$ and *Chn1*$^{KO/KO}$ mice had different phenotypes, confirming that the L20F human amino acid substitution was not loss-of-function and demonstrating both loss and gain of α2-chimaerin function caused defects in abducens development.

The Chn1$^{KI/KI}$ *oculomotor nerve aberrantly innervates the lateral rectus muscle*. Autopsy and electromyographic studies of individuals with DRS suggest that a subpopulation of oculomotor axons ectopically innervate the lateral rectus in the absence of the abducens nucleus and nerve (5–7), leading to the observed eye movement phenotypes. To examine this model further, we crossed *Chn1*$^{KI/KI}$ mice to *Isl*^{MN}-GFP reporter mice — an allele of the ISL1 transcrip-

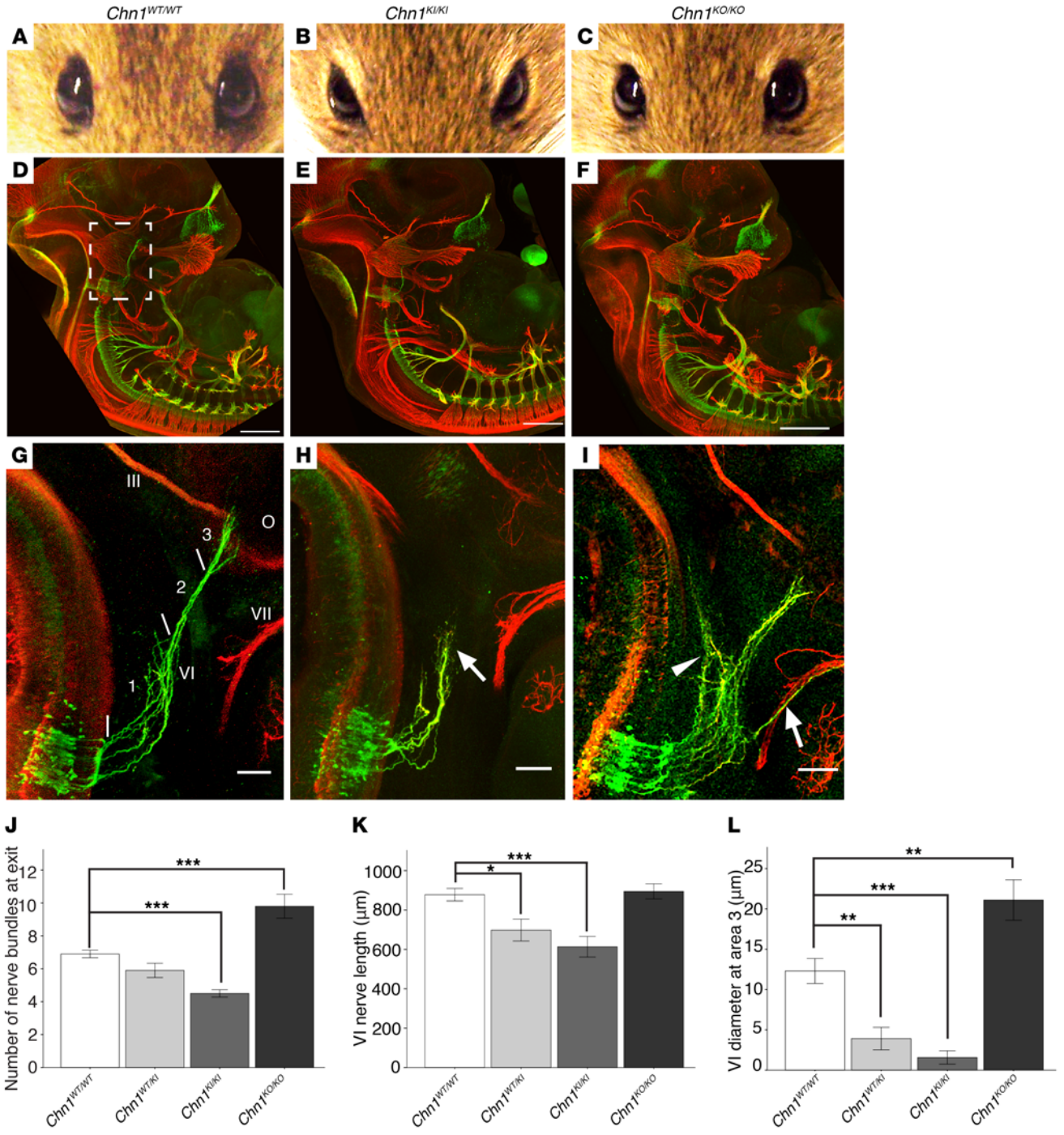

Figure 1. *Chn1*^{KI} mutations are gain-of-function and alter abducens development. (**A**–**C**) Eyes of *Chn1*$^{WT/WT}$ (**A**), *Chn1*$^{KI/KI}$ (**B**), and *Chn1*$^{KO/KO}$ (**C**) adult mice (*Chn1*$^{WT/WT}$: n = 0/44 affected; *Chn1*$^{WT/KI}$: 61.3% affected, n = 144/186; *Chn1*$^{KI/KI}$: 71.8% affected, n = 28/39; *Chn1*$^{KO/KO}$: n = 0/9 affected). (**D**–**F**) Whole mount neurofilament staining of E11.5 *Chn1*$^{WT/WT}$ (**D**), *Chn1*$^{KI/KI}$ (**E**), and *Chn1*$^{KO/KO}$ (**F**) embryos. Scale bars: 500 μm. White box, enlargement in **G**–**I**. Scale bars: 500 μm. (**G**–**I**) Developing abducens nerve (VI) in E11.5 *Chn1*$^{WT/WT}$ (**G**), *Chn1*$^{KI/KI}$ (**H**), and *Chn1*$^{KO/KO}$ (**I**) embryos. Arrow, stalling region in **H** or aberrant fasciculation with facial nerve (VII) in **I**; arrowhead, dorsally projecting nerve bundles. Area 1, abducens hindbrain exit region; area 2, abducens fasciculation region; area 3, abducens EOM innervation region. III, oculomotor, VI, abducens, VII, facial nerves; O, orbit. Scale bars: 100 μm. (**J**–**L**) Number of abducens nerve bundles immediately after exit from the hindbrain within area 1 (**J**); abducens length measured from hindbrain exit to nerve terminus at the orbit (**K**); and abducens diameter measured at line denoting area 3 (**L**). *Chn1*$^{WT/WT}$: n = 20/20 nerves reach orbit (n = 10 embryos); *Chn1*$^{KI/KI}$: 3/10 nerves reach orbit (n = 5 embryos); *Chn1*$^{KO/KO}$: 10/10 reach orbit, 7/10 nerves fasciculate with the facial nerve (n = 5 embryos). Data represent mean ± SEM; $^{*}P < 0.05$, $^{**}P < 0.01$, $^{***}P < 0.001$, 1-way ANOVA with Tukey's test. Red, neurofilament; green, *Hb9*-GFP (26).

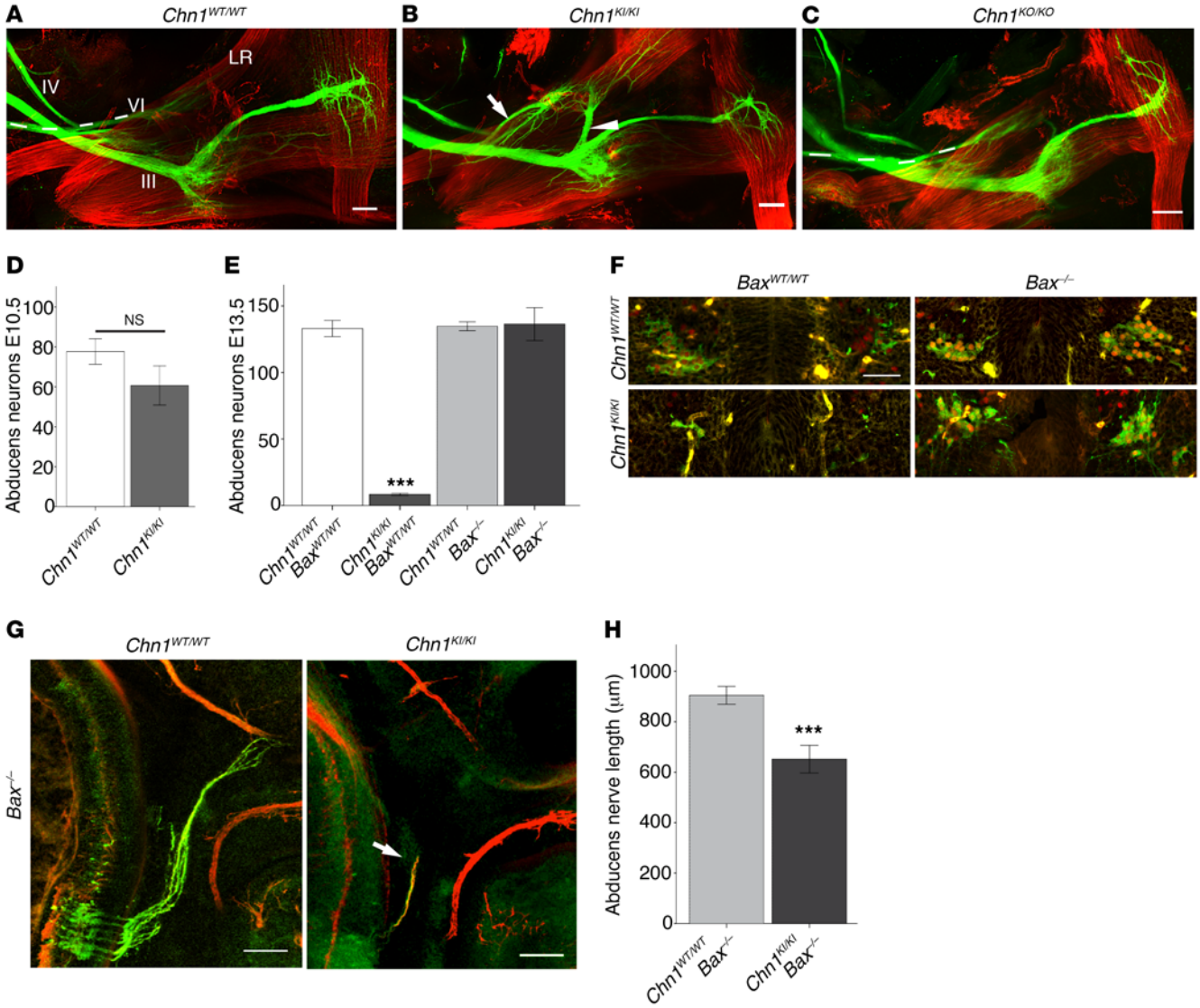

Figure 2. Oculomotor nerve misinnervates lateral rectus muscle, and abducens motor neurons undergo apoptosis following abducens nerve stalling in *Chn1*$^{KI/KI}$ mice. (**A**–**C**) Inferior view of EOM innervation in E16.5 *Chn1*$^{WT/WT}$ (**A**; n = 8 orbits), *Chn1*$^{KI/KI}$ (**B**; n = 7 orbits), and *Chn1*$^{KO/KO}$ embryos (**C**; n = 5 orbits). III, oculomotor; IV, trochlear; VI, abducens. LR, lateral rectus muscle; dotted line, abducens; arrow, aberrant branch from division between superior and inferior III; arrowhead, aberrant branch from inferior III branching region; red, smooth muscle actin (EOM); green, *Isl*^{MN}-GFP (28). Scale bars: 100 μm. (**D**) Number of E10.5 abducens motor neurons in *Chn1*$^{WT/WT}$ and *Chn1*$^{KI/KI}$ embryos. n = 3 embryos; P = 0.231, 2-tailed t test. (**E**) Number of E13.5 abducens motor neurons for the indicated genotypes. n = 3 embryos each; ***$P \le 0.001$, 1-way ANOVA with Tukey's test. (**F**) Representative images of *Hb9*-GFP abducens motor neurons at E13.5 in indicated genotypes; red, ISL1; green, *Hb9*-GFP. Scale bar: 50 μm. (**G**) Whole mount staining of E11.5 *Chn1*$^{WT/WT}$ *Bax*$^{-/-}$ and *Chn1*$^{KI/KI}$ *Bax*$^{-/-}$ embryos. Red, neurofilament; green, *Hb9*-GFP; arrow, abducens nerve stalling. Scale bars: 100 μm. (**H**) Abducens length measurements in whole mount *Chn1*$^{WT/WT}$ *Bax*$^{-/-}$ (n = 16 nerves, 8 embryos) and *Chn1*$^{KI/KI}$ *Bax*$^{-/-}$ embryos (n = 12 nerves, 6 embryos). ***P = 0.001, 2-tailed t test. Graphs represent mean ± SEM.

tion factor gene fused to GFP and tagged with a Ras farnysylation sequence for membrane localization (28) — in order to visualize all cranial motor nuclei and nerve projections and determine whether *Chn1*$^{KI/KI}$ mice exhibit misinnervation by the oculomotor nerve.

In WT embryos, the abducens nerve crossed the oculomotor nerve in close proximity to the lateral rectus prior to its innervation (Figure 2A). The abducens nerve was absent from the orbit in E16.5 *Chn1*$^{KI/KI}$ embryos, consistent with primary stalling rather than delayed outgrowth as the cause of the initial lateral rectus innervation deficit (Figure 2B). While the oculomotor nerve had a normal trajectory to the orbit (Figure 1, D and E, and Supplemental Videos 1 and 2), the lateral rectus was subsequently innervated by one or two aberrant oculomotor nerve branches arising at established oculomotor growth cone decision regions (27): the proximal branch formed from the superior oculomotor nerve division branch-point off the main oculomotor trunk, while the distal branch arose from the inferior oculomotor nerve division branch-point to the medial rectus, inferior rectus, and inferior oblique muscles (Figure 2B). Thus, the oculomotor nerve provides compensatory misinnervation to the lateral rectus in the absence of the abducens nerve, confirming human autopsy and electromyographic data. In *Chn1*$^{KO/KO}$ embryos, the lateral rectus received innervation from the abducens nerve, and there was no stalling or aberrant branching of the oculomo-

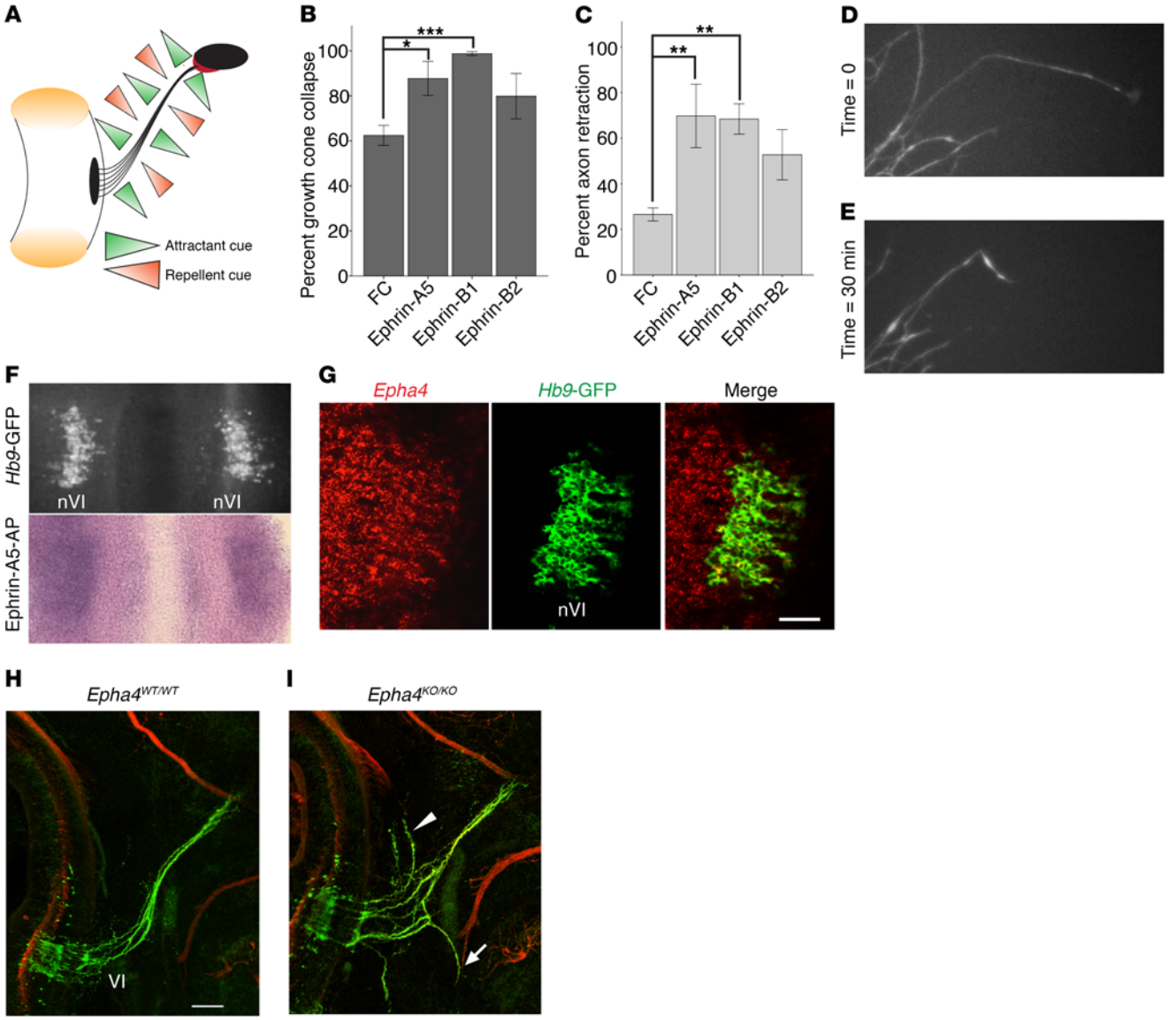

Figure 3. EphA4 is required for normal abducens nerve development. (**A**) Model of balanced WT attractant and repellent guidance cues surrounding developing abducens nerve. Left: hindbrain and black abducens nucleus, right: black orbit and red EOM; left and right connected by abducens nerve in black. Green triangles, attractant cues; orange triangles, repellent cues. (**B** and **C**) Percentage of WT axons in abducens explants exhibiting growth cone collapse (**B**) and axon shaft retraction (**C**) after addition of FC, ephrin-A5, ephrin-B1, or ephrin-B2 ($n \geq 95$ axons from ≥3 experiments for each cue). $^{*}P < 0.05$, $^{**}P < 0.01$, $^{***}P < 0.001$, 1-way ANOVA with Tukey's test; data represent mean ± SEM. (**D** and **E**) Images of abducens growth cones before (**D**) and after (**E**) addition of 200 ng/ml ephrin-A5. (**F**) Ephrin-A5–AP binding to bilateral E11.5 WT abducens nuclei (nVI) in an open-book hindbrain preparation. Top: *Hb9*-GFP–positive abducens nuclei before assay; bottom: ephrin-A5–AP binding to same tissue; $n = 2$. (**G**) *Epha4* (red) and *Hb9*-GFP (green) fluorescence ISH on sagittal section of E11.5 WT abducens nucleus. Scale bar: 50 μm. (**H** and **I**) Whole mount neurofilament staining in E11.5 $Epha4^{WT/WT}$ (**H**) and $Epha4^{KO/KO}$ (**I**) embryos. $n = 5$ embryos; arrow, misprojection with facial nerve; arrowhead, dorsal projections to hindbrain; red, neurofilament; green, *Hb9*-GFP. Scale bar: 100 μm.

tor nerve (Figure 2C); thus, α2-chimaerin is not necessary for final target EOM innervation.

$Chn1^{KI/KI}$ abducens motor neurons undergo apoptosis following abducens nerve stalling. Since the abducens nerve stalls and fails to innervate the lateral rectus in $Chn1^{KI/KI}$ mice, we predicted abducens motor neurons would undergo subsequent apoptosis due to lack of trophic support. Indeed, while the number of $Chn1^{KI/KI}$ abducens motor neurons was not significantly different from WT at E10.5 immediately prior to abducens stalling (Figure 2D), the number was greatly reduced compared with WT by E13.5, 2 days after the abducens phenotype was observed (Figure 2, E and F). To determine whether abducens stalling is primary and independent of subsequent cell death, we crossed $Chn1^{KI/KI}$ mice to $Bax^{-/-}$ mice, thus inhibiting apoptosis during embryogenesis. Abducens motor neuron number was comparable to WT in E13.5 $Chn1^{KI/KI}$ $Bax^{-/-}$ embryos (Figure 2, E and F), yet we observe similar abducens nerve stalling in E11.5 $Chn1^{KI/KI}$ $Bax^{-/-}$ and $Chn1^{KI/KI}$ embryos (Figure 2, G and H, and Figure 1H). Inhibiting apoptosis did not enable abducens nerve innervation of the lateral rectus during later development, as E16.5 $Chn1^{KI/KI}$ $Bax^{-/-}$ embryos lacked abducens nerves in the orbital area and displayed oculomotor misinnervation of the lateral rectus similar to that seen in $Chn1^{KI/KI}$ embryos (Supplemental Figure 2, K and

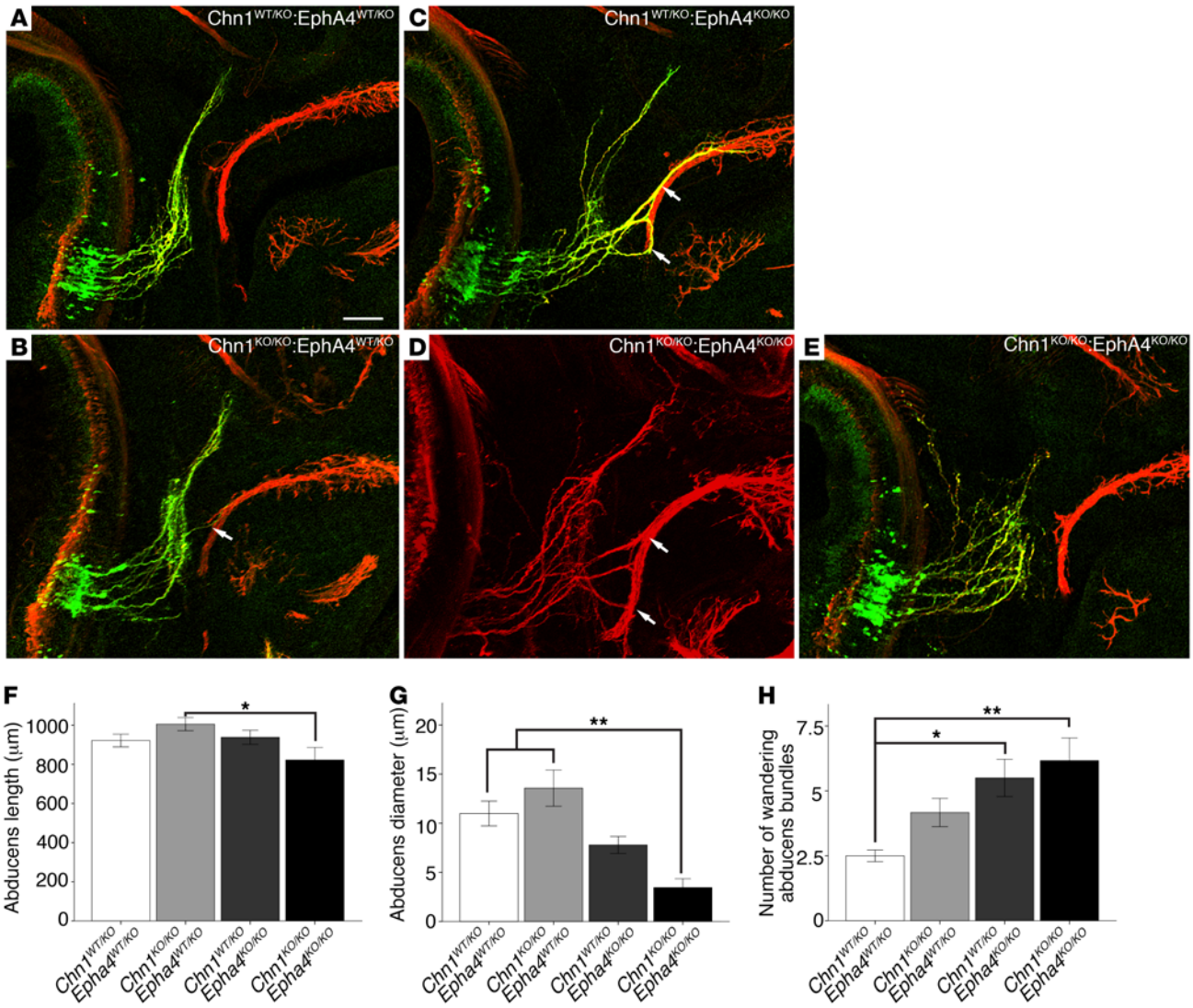

Figure 4. *Chn1*$^{KO/KO}$ *Epha4*$^{KO/KO}$ embryos display reduced abducens nerve diameter and enhanced nerve wandering. (**A**–**E**) Whole mount staining of E11.5 abducens nerves in *Chn1*$^{WT/KO}$ *Epha4*$^{WT/KO}$ (**A**; n = 3 embryos), *Chn1*$^{KO/KO}$ *Epha4*$^{WT/KO}$ (**B**; n = 4 embryos), *Chn1*$^{WT/KO}$ *Epha4*$^{KO/KO}$ (**C**; n = 4 embryos), and *Chn1*$^{KO/KO}$ *Epha4*$^{KO/KO}$ (**D** and **E**; n = 5 embryos) embryos. Arrows, abducens nerve fasciculation with buccal branch of facial nerve; 3/5 *Chn1*$^{KO/KO}$ *Epha4*$^{KO/KO}$ E11.5 embryos have abducens phenotypes similar to that in **D** and 2/5 are similar to that in **E**. Scale bar: 100 μm. (**F**–**H**) Abducens nerve length from hindbrain exit to most distal projection (**F**); abducens diameter at orbit (**G**); and number of wandering abducens nerve bundles (**H**). *P < 0.05, **P < 0.01, 1-way ANOVA with Tukey's test; data represent mean ± SEM.

L, and Figure 2B). These data support primary abducens nerve stalling at E11.5, failure of lateral rectus target innervation, and subsequent secondary abducens motor neuron apoptosis by E13.5.

Epha4$^{KO/KO}$ *and Chn1*$^{KO/KO}$ *mice exhibit a similar abducens phenotype*. There is strong in vivo and in vitro evidence that α2-chimaerin acts downstream of EphA4 in developing upper and lower motor neurons to elicit growth cone collapse (12–15, 29). Corticospinal and central pattern generator neuronal tracts in both *Chn1*$^{KO/KO}$ and *Epha4*$^{KO/KO}$ mice aberrantly cross the spinal cord midline, as their axons lack responsiveness to ephrin midline repellents (12, 14, 15, 21). We hypothesized that gain-of-function *Chn1*^{KI} mutations could act downstream of EphA4 to increase repulsion to ephrins and further enhance growth cone collapse (Figure 3A). We used abducens explant cultures to assess growth cone collapse and axon retraction in response to ephrin-A and –B guidance factors in vitro. Abducens neurons exhibited significant growth cone collapse and axon retraction upon bath application of recombinant ephrin-A5 and ephrin-B1 and trended toward collapse and retraction with ephrin-B2 (Figure 3, B–E, and Supplemental Video 4).

Using an ephrin-A5–AP binding assay, we found that ephrin-A5 bound to the abducens nucleus at E11.5 (Figure 3F). We focused specifically on the involvement of EphA4 in ephrin-mediated binding and repulsion because α2-chimaerin is reported to act downstream of EphA4 and not EphB isoforms (13, 29). In situ hybridization (ISH) in E11.5 embryos revealed *Epha4* expression in abducens motor neurons (Figure 3G). We reasoned that if ephrin/EphA4 signaling is the main regulator of abducens development upstream of α2-chimaerin, we could expect *Epha4*$^{KO/KO}$ and *Chn1*$^{KO/KO}$

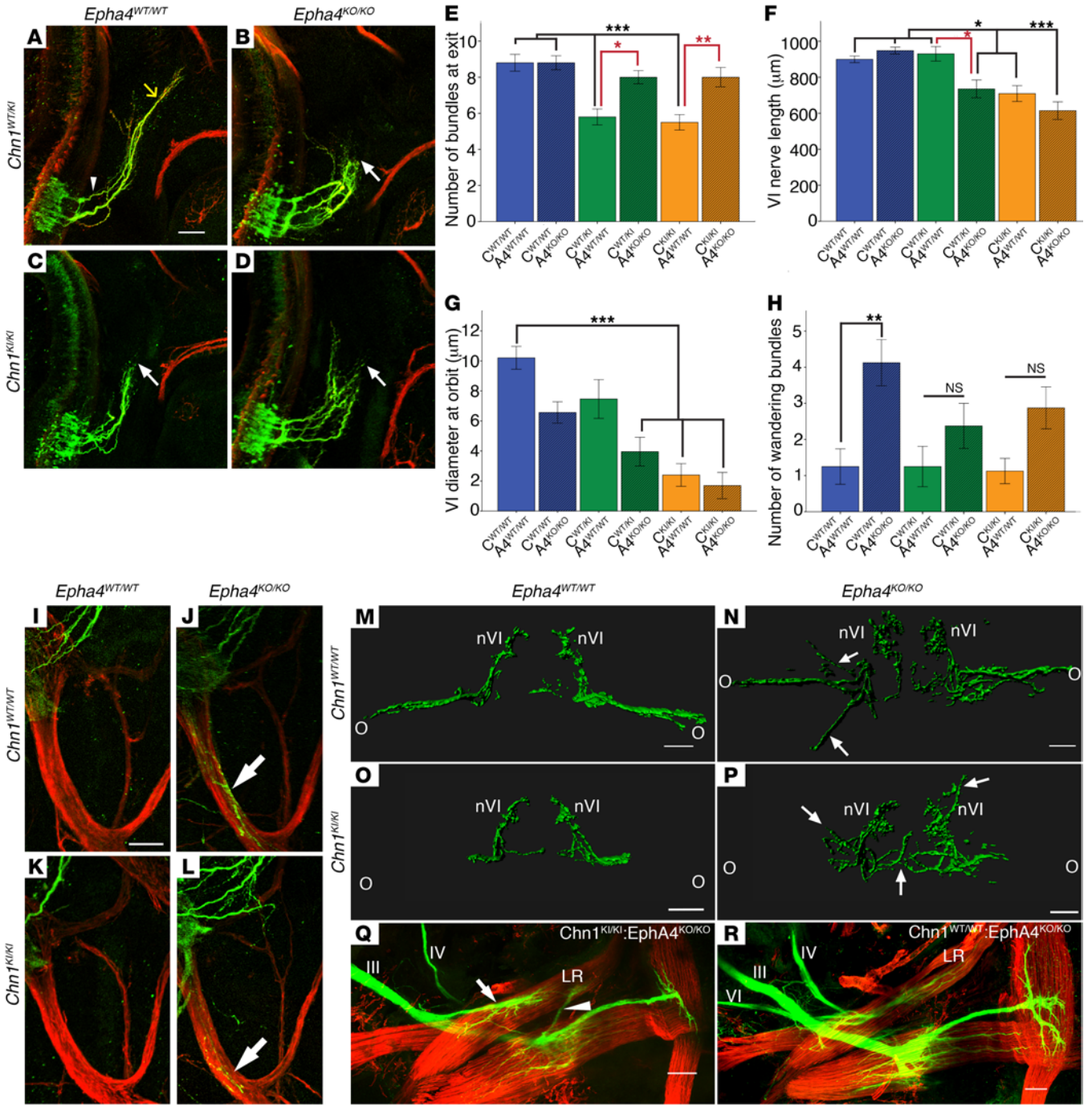

Figure 5. Complex genetic interaction between EphA4 and α2-chimaerin in abducens nerve development. (**A**–**D**) Whole mount staining of E11.5 abducens nerves in *Chn1*$^{WT/KI}$ *Epha4*$^{WT/WT}$ (**A**), *Chn1*$^{WT/KI}$ *Epha4*$^{KO/KO}$ (**B**), *Chn1*$^{KI/KI}$ *Epha4*$^{WT/WT}$ (**C**), and *Chn1*$^{KI/KI}$ *Epha4*$^{KO/KO}$ (**D**) embryos. *n* = 10 nerves (5 embryos) for all genotypes; arrowhead, exited abducens nerve bundles counted in **E**; white arrow, location of abducens stalling measured in **F**; yellow arrow, location of abducens diameter at orbit measured in **G**; red, neurofilament; green, *Hb9*-GFP. (**E**–**H**) Number of abducens nerve bundles at hindbrain exit (**E**); abducens length from hindbrain exit to most distal projection (**F**); abducens diameter at orbit (**G**); and number of wandering abducens nerve bundles (**H**) as measured from transverse images in **M**–**P**. **P* < 0.05, ***P* < 0.01, ****P* < 0.001, 1-way ANOVA with Tukey's test; data represent mean ± SEM. C, *Chn1*; A4, *Epha4*. (**I**–**L**) Abducens fasciculation with mandibular and cervical branches of the facial nerve in E11.5 *Chn1*$^{WT/WT}$ *Epha4*$^{KO/KO}$ (**J**) and *Chn1*$^{KI/KI}$ *Epha4*$^{KO/KO}$ (**L**) embryos. Arrows, *Hb9*-GFP abducens axons tracking with red (neurofilament) facial nerve; *n* = 5 embryos per genotype. (**M**–**P**) Transverse view of bilateral abducens nerves in E11.5 *Chn1*$^{WT/WT}$ *Epha4*$^{WT/WT}$ (**M**), *Chn1*$^{WT/WT}$ *Epha4*$^{KO/KO}$ (**N**), *Chn1*$^{KI/KI}$ *Epha4*$^{WT/WT}$ (**O**), *Chn1*$^{KI/KI}$ *Epha4*$^{KO/KO}$ (**P**) embryos. Green, *Hb9*-GFP; *n* = 4 embryos per genotype; nVI, abducens nucleus; O, orbit; arrows, wandering abducens nerve bundles. (**Q** and **R**) Orbital imaging of oculomotor (III), trochlear (IV), and abducens (VI) nerves innervating EOM at E16.5. LR, lateral rectus. *Chn1*$^{KI/KI}$ *Epha4*$^{KO/KO}$ (**Q**): *n* = 5/5 orbits without abducens nerve and with aberrant oculomotor nerve branching to LR; arrows, aberrant oculomotor branching toward LR. *Chn1*$^{WT/WT}$ *Epha4*$^{KO/KO}$ (**R**): *n* = 4/6 orbits with normal LR innervation and 2/6 with thin abducens nerve and minor aberrant oculomotor nerve branching. Red, actin smooth muscle; green, *Isl*^{MN}-GFP. All scale bars: 100 μm.

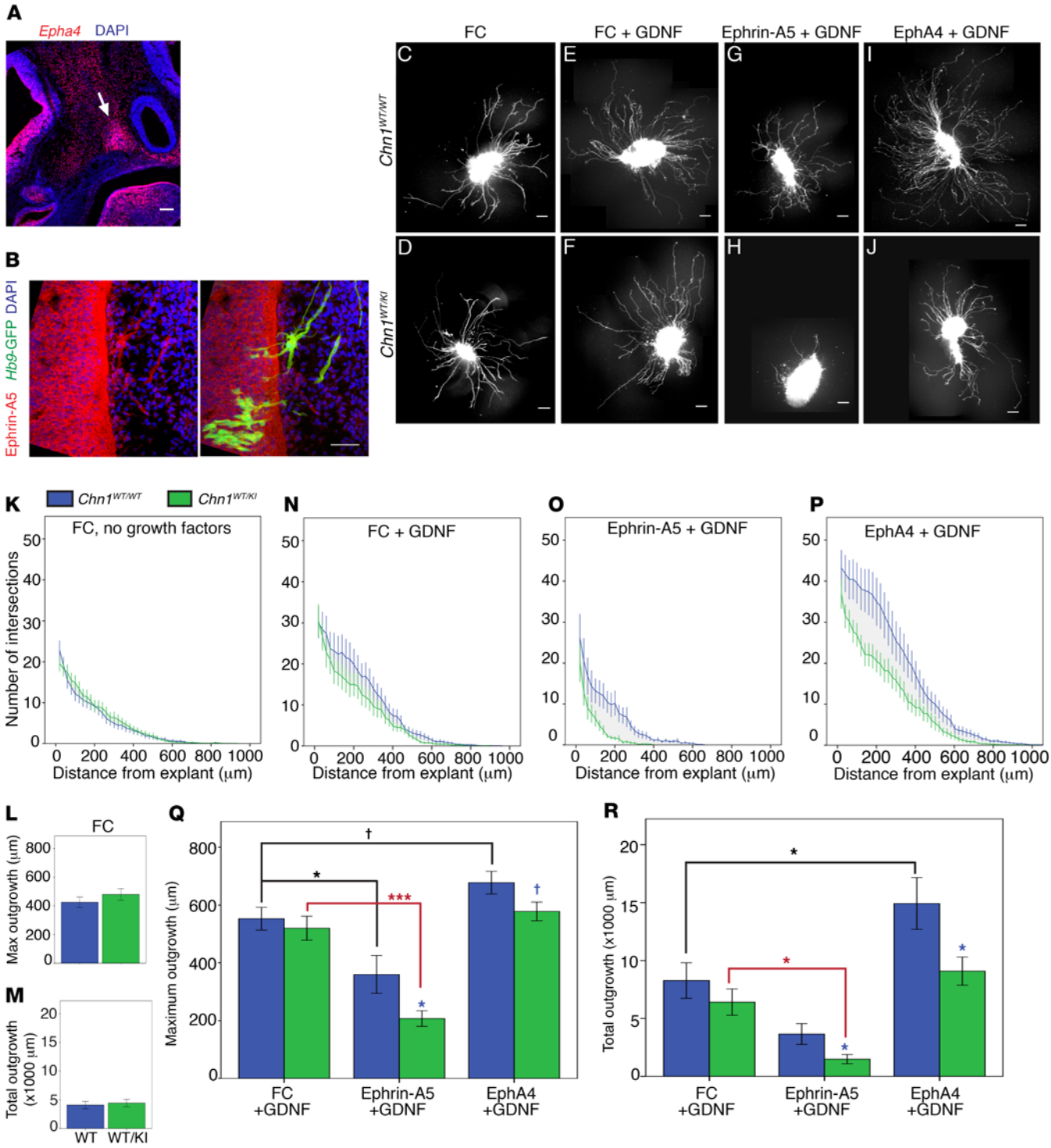

Figure 6. *Chn1*^{KI} alters ephrin forward and reverse signaling in abducens neurons. (**A**) Sagittal E11.5 WT embryo with *Epha4* localization (red) in mesenchyme and EOM anlage. Arrow, EOM anlage; blue, DAPI. Scale bar: 100 μm. (**B**) Sagittal E11.5 WT embryo with ephrin-A5 protein localization in abducens nerve bundles. Red, ephrin-A5; green, *Hb9*-GFP–positive abducens projections; blue, DAPI. Scale bar: 50 μm; $n = 2$. (**C**–**J**) Sample images of E11.5 *Chn1*$^{WT/WT}$ (top row) and *Chn1*$^{WT/KI}$ (bottom row) *Hb9*-GFP–positive abducens nucleus explants grown in 50 ng/ml FC without growth factor (**C** and **D**) or with 50 ng/ml FC+25 ng/ml GDNF (**E** and **F**), 50 ng/ml ephrin-A5+25 ng/ml GDNF (**G** and **H**), or 1 μg/ml EphA4+25 ng/ml GDNF (**I** and **J**). Scale bars: 100 μm. (**K**–**M**) Sholl analysis of E11.5 *Chn1*$^{WT/WT}$ (blue, $n = 28$ explants) and *Chn1*$^{WT/KI}$ (green, $n = 23$ explants) abducens explants cultured in 50 ng/ml FC (**K**: 7 experiments). (**L** and **M**) Quantification of average maximum outgrowth (**L**) and total outgrowth (**M**) from **K**. (**N**–**R**) Sholl analysis of E11.5 *Chn1*$^{WT/WT}$ (blue) and *Chn1*$^{WT/KI}$ (green) abducens explants cultured in 50 ng/ml FC with 25 ng/ml GDNF (*Chn1*$^{WT/WT}$: $n = 13$, *Chn1*$^{WT/KI}$: $n = 7$, 4 experiments) (**N**); 50 ng/ml ephrin-A5 with 25 ng/ml GDNF (*Chn1*$^{WT/WT}$: $n = 11$, *Chn1*$^{WT/KI}$: $n = 13$, 5 experiments) (**O**); and 1 μg/ml EphA4 with 25 ng/ml GDNF (*Chn1*$^{WT/WT}$: $n = 19$, *Chn1*$^{WT/KI}$: $n = 19$, 6 experiments) (**P**). (**Q** and **R**) Quantification of average maximum outgrowth (**Q**) and total outgrowth (**R**) from **N**–**P**. †$P < 0.07$, *$P < 0.05$, ***$P < 0.001$; black asterisks, comparisons within *Chn1*$^{WT/WT}$ explant between three cues; red asterisks, comparisons within *Chn1*$^{WT/KI}$ between cues, 1-way ANOVA with Dunnett's test; blue asterisks, comparisons between *Chn1*$^{WT/WT}$ and *Chn1*$^{WT/KI}$ within each cue by unpaired 2-tailed *t* test.

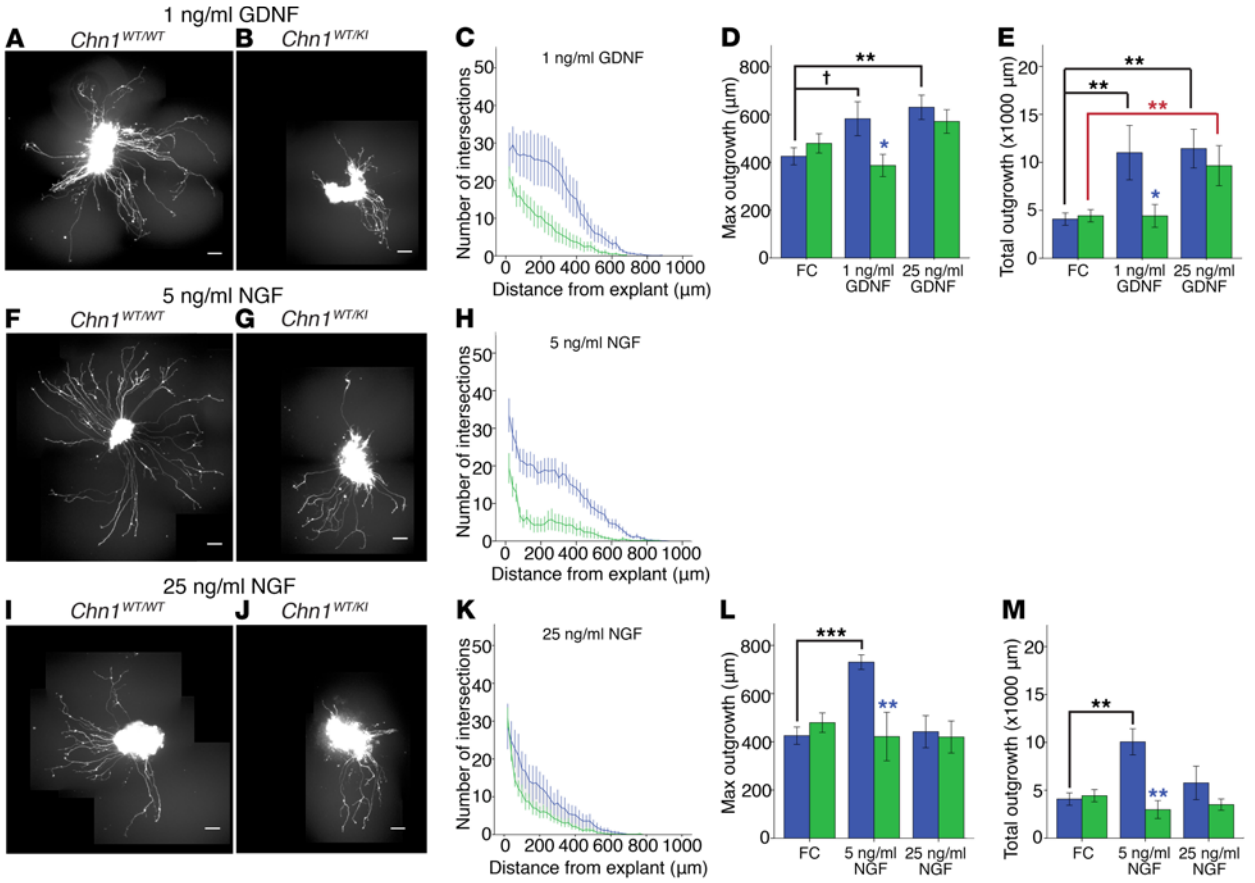

Figure 7. Ephrin reverse signaling in abducens neurons may involve Ret and p75^{NTR} co-receptors. (**A**–**E**) Sholl analysis of E11.5 *Chn1*$^{WT/WT}$ (**A**) and *Chn1*$^{WT/KI}$ (**B**) abducens explants cultured in 1 ng/ml GDNF (blue: *Chn1*$^{WT/WT}$, *n* = 13, green: *Chn1*$^{WT/KI}$, *n* = 15, 4 experiments) (**C**). (**D** and **E**) Quantification of average maximum outgrowth (**D**) and total outgrowth (**E**) from **C**. (**F**–**M**) Sholl analysis of E11.5 *Chn1*$^{WT/WT}$ (**F**) and *Chn1*$^{WT/KI}$ (**G**) abducens explants cultured in 5 ng/ml NGF (*Chn1*$^{WT/WT}$: *n* = 11, *Chn1*$^{WT/KI}$: *n* = 8, 3 experiments) (**H**); and *Chn1*$^{WT/WT}$ (**I**) and *Chn1*$^{WT/KI}$ (**J**) abducens explants cultured in 25 ng/ml NGF (*Chn1*$^{WT/WT}$: *n* = 10, *Chn1*$^{WT/KI}$: *n* = 10, 3 experiments) (**K**). (**L** and **M**) Quantification of average maximum outgrowth (**L**) and total outgrowth (**M**) from **H** and **K**. Scale bars: 100 μm. $^{\dagger}P < 0.07$, $^{*}P < 0.05$, $^{**}P < 0.01$, $^{***}P < 0.001$. Black cross and asterisks, comparison within *Chn1*$^{WT/WT}$ between cues by 1-way ANOVA with Dunnett's test; red asterisks, comparison within *Chn1*$^{WT/KI}$ between cues by 1-way ANOVA with Dunnett's test; blue asterisks, comparisons between *Chn1*$^{WT/WT}$ and *Chn1*$^{WT/KI}$ within each cue by unpaired 2-tailed *t* test.

embryos to have a similar abducens phenotype. We crossed *Epha4*$^{fl/fl}$ (30) to *E2A-Cre* mice (31) to create a germline knockout of EphA4 (*Epha4*$^{KO/KO}$; Supplemental Figure 3A). Indeed, whole mount neurofilament imaging of *Epha4*$^{KO/KO}$ embryos revealed abducens nerve wandering strikingly similar to that in *Chn1*$^{KO/KO}$ embryos (Figure 3, H and I, Figure 1I, and Supplemental Video 5). There were, however, subtle phenotypic differences: *Epha4*$^{KO/KO}$ abducens nerves appeared less defasciculated than *Chn1*$^{KO/KO}$; aberrant fascicles wandered more; and some aberrant fascicles tracked with the mandibular and cervical branches of the facial nerve, rather than the buccal branch. Moreover, E13.5 *Epha4*$^{KO/KO}$ embryos had approximately half the number of abducens motor neurons than WT embryos (Supplemental Figure 3, B and C), consistent with survival of only those motor neurons whose axons successfully reached the EOM anlage within area 3. These results confirm that EphA4 signaling is important for proper abducens nerve development and may act within an α2-chimaerin–mediated pathway.

Abducens nerve phenotype is slightly altered in Chn1$^{KO/KO}$ *Epha4*$^{KO/KO}$ *embryos compared with embryos harboring individual Chn1*$^{KO/KO}$ *or Epha4*$^{KO/KO}$ *alleles*. To further investigate potential pathway interactions between *Chn1* and *Epha4*, we generated and examined *Chn1*$^{WT/KO}$ *Epha4*$^{WT/KO}$, *Chn1*$^{WT/KO}$ *Epha4*$^{KO/KO}$, *Chn1*$^{KO/KO}$ *Epha4*$^{WT/KO}$, and *Chn1*$^{KO/KO}$ *Epha4*$^{KO/KO}$ double mutant embryos. *Chn1*$^{WT/KO}$ *Epha4*$^{WT/KO}$ embryos appeared like WT embryos (Figure 4A and Figure 1G); *Chn1*$^{KO/KO}$ *Epha4*$^{WT/KO}$ embryos appeared like *Chn1*$^{KO/KO}$ embryos (Figure 4B and Figure 1I); and *Chn1*$^{WT/KO}$ *Epha4*$^{KO/KO}$ embryos appeared like *Epha4*$^{KO/KO}$ embryos (Figure 4C and Figure 3I) — demonstrating that haploinsufficiency of both pathways is not sufficient to elicit a phenotype, and haploinsufficiency of either allele combined with a knockout of the other allele does not alter the knockout phenotype. *Chn1*$^{KO/KO}$ *Epha4*$^{WT/KO}$ and *Chn1*$^{WT/KO}$ *Epha4*$^{KO/KO}$ embryos were not statistically different from one another, and a subset of abducens nerve bundles consistently reached the orbit (Figure 4, B, C, and F–H). There were, however, trends toward increased wandering and reduced abducens diameter in *Chn1*$^{WT/KO}$ *Epha4*$^{KO/KO}$ compared with *Chn1*$^{KO/KO}$ *Epha4*$^{WT/KO}$ embryos (Figure 4, G and H), which recapitulated the subtle phenotypic differences between *Chn1*$^{KO/KO}$ and *Epha4*$^{KO/KO}$ embryos (Figure 1I and Figure 3I).

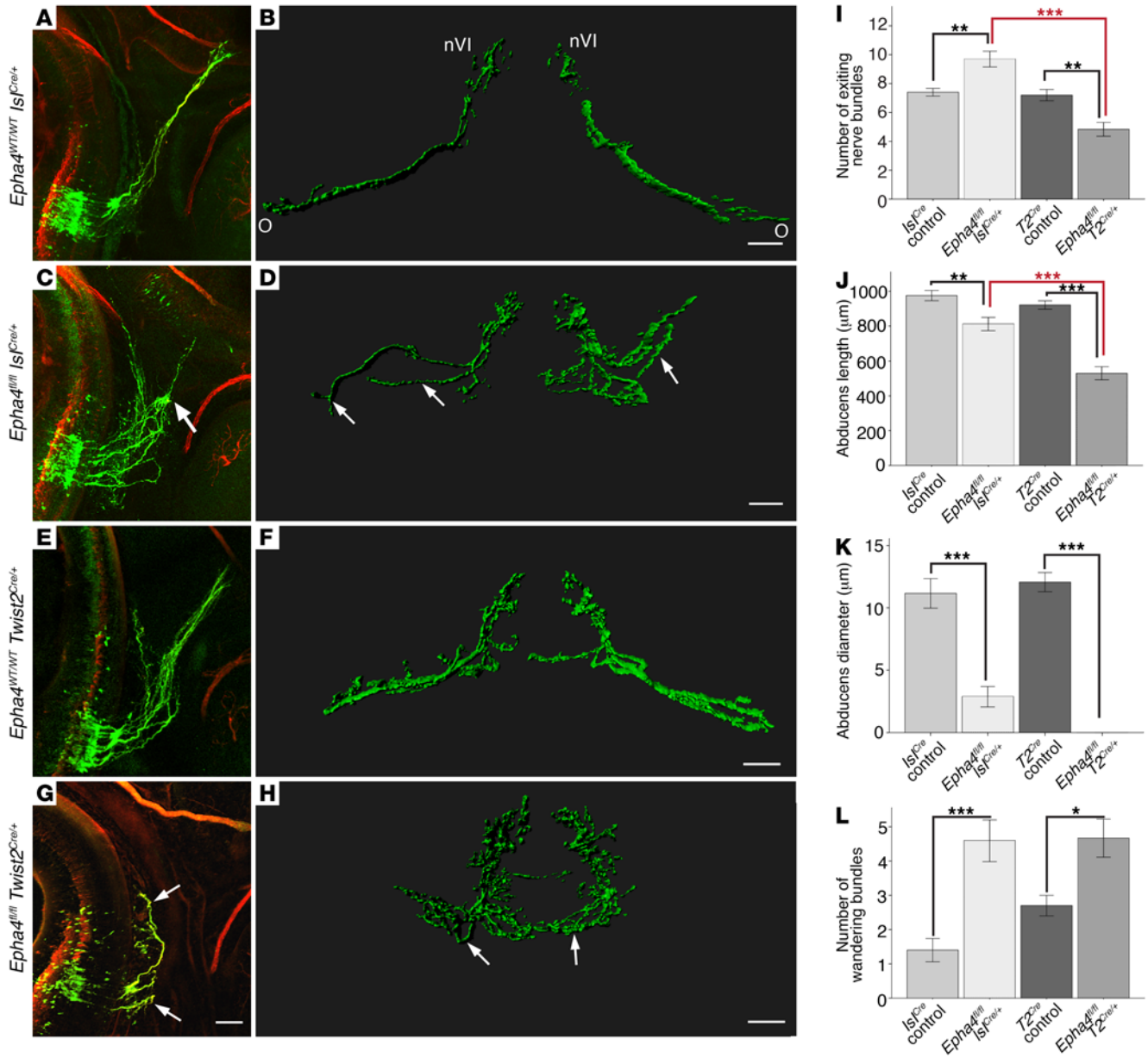

Figure 8. Bidirectional EphA4 signaling is critical for normal abducens development. (**A** and **B**) E11.5 *Epha4*$^{WT/WT}$ *Isl*$^{Cre/+}$ abducens nerve in sagittal (**A**) and Imaris surface-rendered transverse view (**B**); *n* = 5 embryos. (**C** and **D**) *Epha4*$^{fl/fl}$ *Isl*$^{Cre/+}$ abducens nerve in sagittal (**C**) and transverse view (**D**); arrows indicate wandering within area 2; *n* = 5 embryos. (**E** and **F**) *Epha4*$^{WT/WT}$ *Twist2*$^{Cre/+}$ abducens nerve in sagittal (**E**) and transverse views (**F**); *n* = 5 embryos. (**G** and **H**) *Epha4*$^{fl/fl}$ *Twist2*$^{Cre/+}$ abducens nerve in sagittal (**G**) and transverse views (**H**); arrows, stalled nerve bundles after exit from area 1; *n* = 3 embryos. nVI, abducens nucleus; O, orbit; red, neurofilament; green, *Hb9*-GFP. Scale bars: 100 μm. (**I**–**L**) Number of exited abducens nerve bundles (**I**), abducens nerve length (**J**), abducens diameter at orbit (**K**), and wandering abducens nerve bundles (**L**) for indicated genotypes; **P* < 0.05, ***P* < 0.01, ****P* < 0.001, 1-way ANOVA with Tukey's test; data represent mean ± SEM. *T2*^{Cre}, *Twist2*^{Cre}.

The double homozygous *Chn1*$^{KO/KO}$ *Epha4*$^{KO/KO}$ embryos were qualitatively most similar to *Epha4*$^{KO/KO}$ and *Chn1*$^{WT/KO}$ *Epha4*$^{KO/KO}$ embryos (Figure 4, C–E). While there were no statistically significant differences between *Chn1*$^{KO/KO}$ *Epha4*$^{KO/KO}$ and *Chn1*$^{WT/KO}$ *Epha4*$^{KO/KO}$ embryos (Figure 4, F–H), there was a trend toward reduced abducens nerve diameter at the orbit, which appeared to result from a higher incidence of orbital innervation failure (2 of 5 embryos, Figure 4E). Compared with *Chn1*$^{KO/KO}$ *Epha4*$^{WT/KO}$ embryos, the double mutants had significantly reduced abducens nerve length and diameter at the orbit (Figure 4, F and G). Thus, while α2-chimaerin and EphA4 share a common pathway, the mild differences between the single mutants and mild alterations in the phenotype of the double mutant compared with the single mutants suggest that additional pathways either upstream of α2-chimaerin and/or downstream of EphA4 may also be involved in abducens nerve development.

Chn1$^{KI/KI}$*Epha4*$^{KO/KO}$ *embryos have normalized abducens nerve exit, increased nerve stalling compared with Chn1*$^{KI/KI}$*, and similar abducens nerve wandering compared with Epha4*$^{KO/KO}$. We next explored the *Chn1*$^{KI/KI}$ abducens nerve in *Chn1*$^{WT/KI}$ *Epha4*$^{KO/KO}$

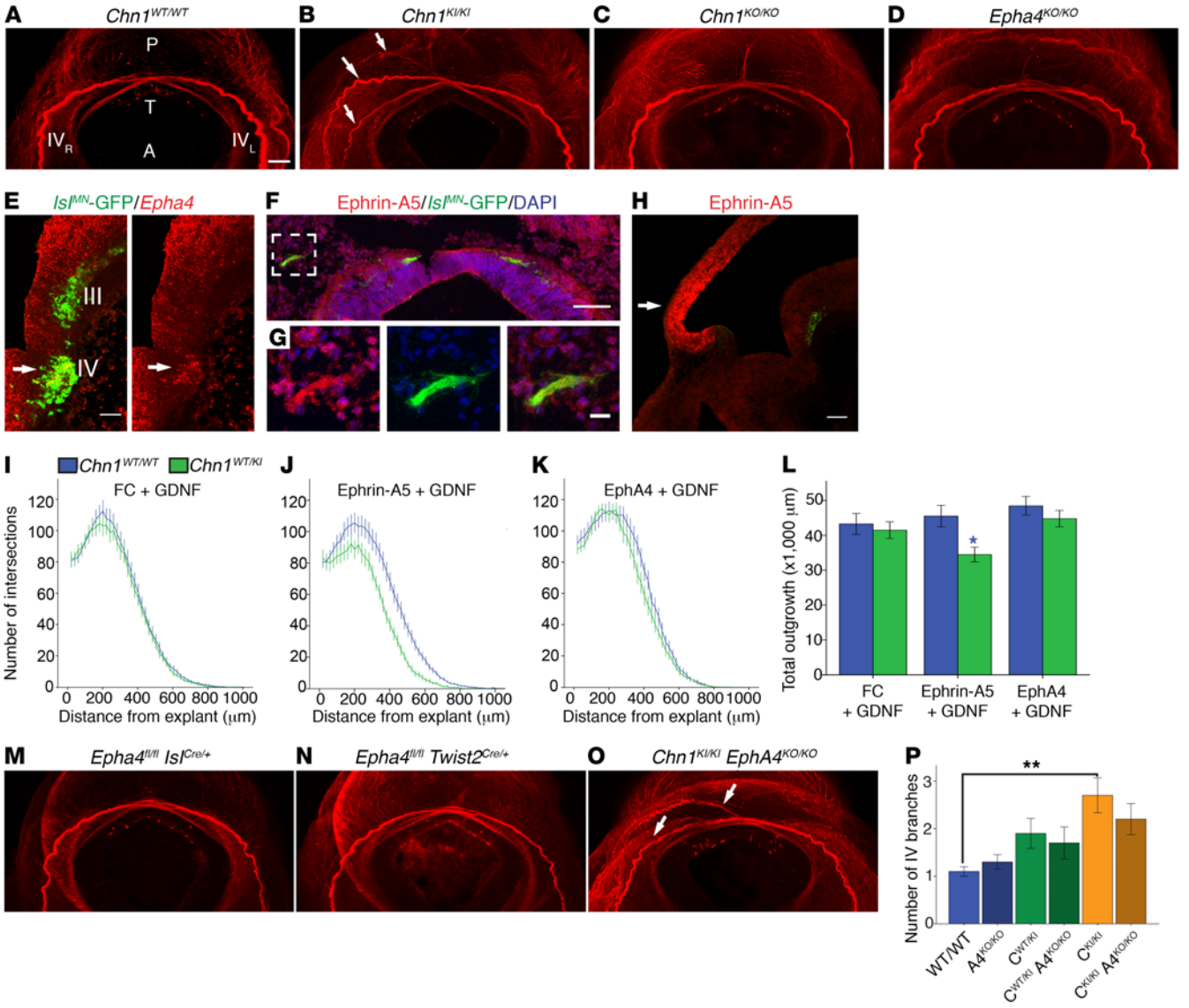

Figure 9. *Chn1*$^{KI/KI}$ trochlear nerve branching abnormalities are unaltered by *Epha4*^{KO} allele. (**A**–**D**) Transverse view of crossing trochlear nerves (IV) in E11.5 *Chn1*$^{WT/WT}$ (**A**; $n = 4$), *Chn1*$^{KI/KI}$ (**B**; $n = 4$), *Chn1*$^{KO/KO}$ (**C**; $n = 4$), and *Epha4*$^{KO/KO}$ (**D**; $n = 4$) embryos. P, posterior; A, anterior; T, tectum; IV_R and IV_L, right and left trochlear nerves; arrows, aberrant trochlear branches; red, neurofilament. Scale bars: 100 μm. (**E**) *Epha4* expression in trochlear nucleus (arrow); red, *Epha4*; green, *Isl*^{MN}-GFP; III, oculomotor; IV, trochlear nuclei. Scale bar: 50 μm. (**F** and **G**) Ephrin-A5 protein in peripheral trochlear axons. Scale bar: 100 μm. White box: enlargement in (**G**) with 20 μm scale bar. Red, ephrin-A5; green, *Isl*^{MN}-GFP; blue, DAPI. (**H**) Ephrin-A5 (red) and *Hb9*-GFP (green) fluorescence ISH on sagittal E11.5 WT brainstem. Arrow, tectum. (**I**–**K**) Sholl analysis of E11.5 *Chn1*$^{WT/WT}$ (blue) and *Chn1*$^{WT/KI}$ (green) trochlear explants cultured in 50 ng/ml FC with 25 ng/ml GDNF (**I**; *Chn1*$^{WT/WT}$: $n = 25$, *Chn1*$^{WT/KI}$: $n = 17$, 4 experiments); 50 ng/ml ephrin-A5 with 25 ng/ml GDNF (**J**; *Chn1*$^{WT/WT}$: $n = 24$, *Chn1*$^{WT/KI}$: $n = 15$, 4 experiments); and 1 μg/ml EphA4 with 25 ng/ml GDNF (**K**; *Chn1*$^{WT/WT}$: $n = 19$, *Chn1*$^{WT/KI}$: $n = 21$, 4 experiments). (**L**) Quantification of total outgrowth (AUC); $^*P < 0.05$; blue asterisk, comparison between *Chn1*$^{WT/WT}$ and *Chn1*$^{WT/KI}$ within each cue by unpaired 2-tailed *t* test. (**M**–**O**) Transverse view of crossing trochlear nerves in E11.5 *Epha4*$^{fl/fl}$ *Isl*$^{Cre/+}$ (**M**; $n = 5$), *Epha4*$^{fl/fl}$ *Twist2*$^{Cre/+}$ (**N**; $n = 3$), and *Chn1*$^{KI/KI}$ *Epha4*$^{KO/KO}$ (**O**; $n = 5$) embryos. Arrows, aberrant trochlear branches; red, neurofilament. (**P**) Quantification of trochlear branching. $^{**}P < 0.01$, 1-way ANOVA with Tukey's test. Four individual images taken with a ×5 objective were tiled to generate the stitched images shown in panels **A**–**D** and **M**–**O**, and scale is as per bar in **A**. Graphs represent mean ± SEM.

or *Chn1*$^{KI/KI}$ *Epha4*$^{KO/KO}$ embryos, anticipating we would find one of several potential phenotypes. First, although mutant α2-chimaerin was not constitutively hyperactive in cortical neurons (Supplemental Figure 1F), it remained possible that mutant α2-chimaerin was constitutively hyperactive in abducens neurons irrespective of receptor activation. Second, it is possible that mutant α2-chimaerin was not constitutively active, but could be recruited to full hyperactivity downstream of a non-EphA4 pathway. Either scenario would be predicted to result in the *Chn1*$^{KI/KI}$ abducens nerve stalling phenotype in the double mutant. Third, if α2-chimaerin were not constitutively active in abducens neurons and EphA4 were the only upstream receptor that activates α2-chimaerin, we would predict to find the *Epha4*$^{KO/KO}$ abducens phenotype in double mutant mice. Finally, if α2-chimaerin were not constitutively active and, in addition to EphA4, a non–EphA4 receptor–meditated pathway were also able to activate mutant α2-chimaerin, we would predict restored abducens outgrowth or potentially a more complex phenotype,

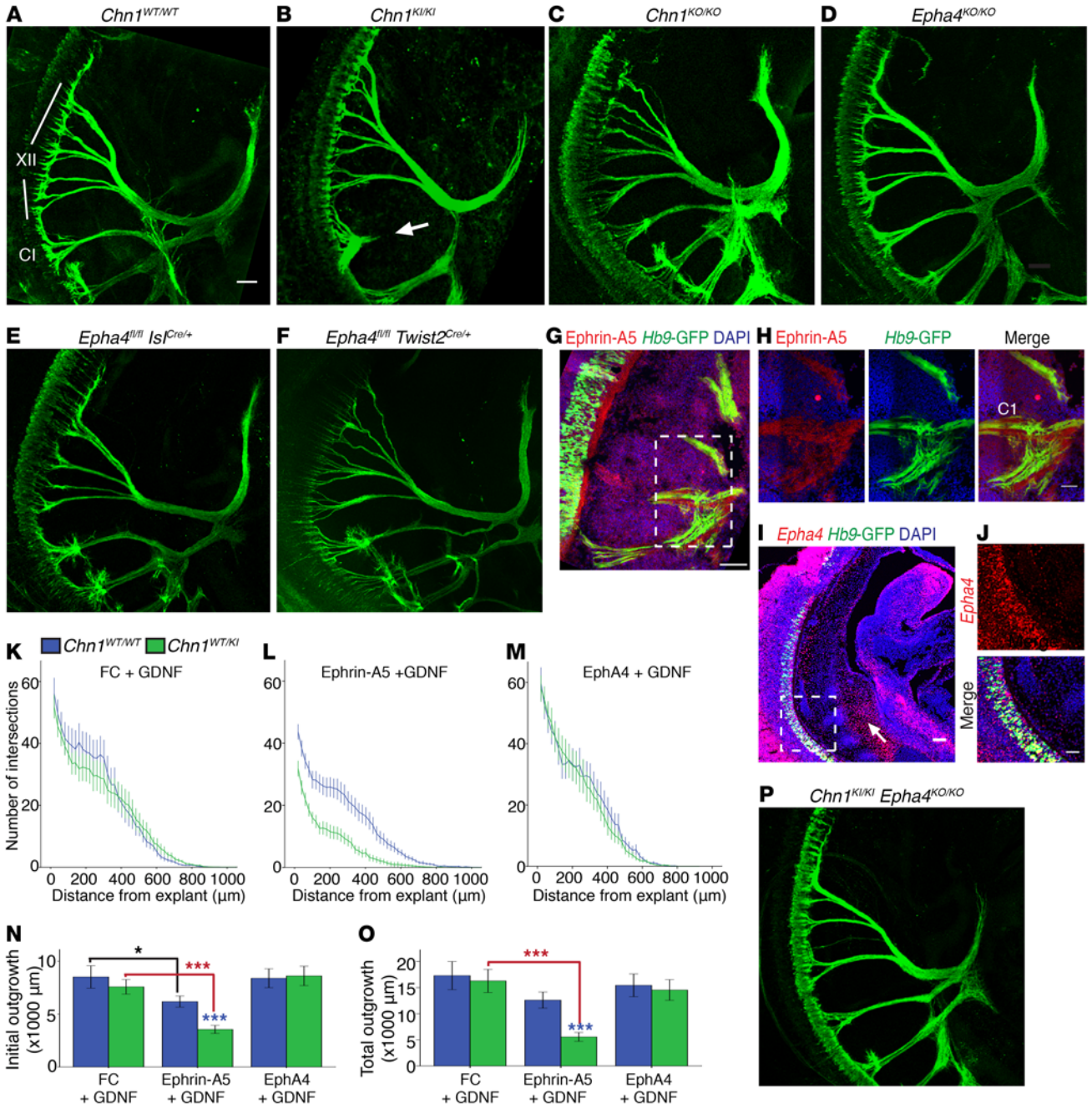

Figure 10. *Chn1*$^{KI/KI}$ embryos exhibit first cervical spinal nerve (C1) projection abnormalities that are reversed by *Epha4*^{KO} allele. (**A**–**F**) C1 projections in E11.5 *Chn1*$^{WT/WT}$ (**A**; $n = 10$), *Chn1*$^{KI/KI}$ (**B**; $n = 5$), *Chn1*$^{KO/KO}$ (**C**; $n = 5$), *Epha4*$^{KO/KO}$ (**D**; $n = 5$), *Epha4*$^{fl/fl}$ *Isl*$^{Cre/+}$ (**E**; $n = 5$), and *Epha4*$^{fl/fl}$ *Twist2*$^{Cre/+}$ (**F**; $n = 3$) embryos. Arrow, direction of C1 dorsal turning toward dermomyotome; green, *Hb9*-GFP; XII, hypoglossal; C1, first cervical spinal segment. Scale bar: 100 μm. (**G**) Ephrin-A5 protein localization in C1 axons and area immediately adjacent to axons. Scale bar: 100 μm; $n = 2$. White box, enlargement in **H**; scale bar: 50 μm; red, ephrin-A5; green, *Hb9*-GFP; blue: DAPI. (**I**) *Epha4* ISH in C1 (box) and mesenchyme surrounding C1 (arrow) in sagittal view of WT E11.5 embryo. Scale bar: 100 μm; $n = 2$. White box, enlargement in **J**; scale bar: 50 μm; red, *Epha4*; green, *Hb9*-GFP; blue, DAPI. (**K**–**M**) Sholl analysis of E11.5 *Chn1*$^{WT/WT}$ (blue) and *Chn1*$^{WT/KI}$ (green) C1 explants cultured in 50 ng/ml FC with 25 ng/ml GDNF (**K**; *Chn1*$^{WT/WT}$: $n = 23$, *Chn1*$^{WT/KI}$: $n = 28$, 4 experiments); 50 ng/ml ephrin-A5 with 25 ng/ml GDNF (**L**; *Chn1*$^{WT/WT}$: $n = 43$, *Chn1*$^{WT/KI}$: $n = 37$, 6 experiments); and 1 μg/ml EphA4 with 25 ng/ml GDNF (**M**; *Chn1*$^{WT/WT}$: $n = 14$, *Chn1*$^{WT/KI}$: $n = 26$, 3 experiments). (**N** and **O**) Quantification of initial outgrowth (**N**; AUC from 0 to 200 μm) and total outgrowth (**O**; total AUC). $^*P < 0.05$, $^{***}P < 0.001$; black asterisk, comparison within *Chn1*$^{WT/WT}$ between cues; red asterisks, comparison within *Chn1*$^{WT/KI}$ between cues by 1-way ANOVA with Dunnett's test; blue asterisks, comparison between *Chn1*$^{WT/WT}$ and *Chn1*$^{WT/KI}$ within each cue by unpaired 2-tailed *t* test. Data represent mean ± SEM. (**P**) C1 projections in E11.5 *Chn1*$^{KI/KI}$ *Epha4*$^{KO/KO}$ embryo; $n = 5$.

depending on the extent of activation and the role each receptor plays in abducens development.

We found that the *Chn1*$^{WT/KI}$ *Epha4*$^{KO/KO}$ or *Chn1*$^{KI/KI}$ *Epha4*$^{KO/KO}$ embryos had different alterations in growth within each developmental area of the abducens nerve (as outlined in Figure 1G), supporting both EphA4- and non–EphA4 receptor–mediated pathways upstream of α2-chimaerin and absence of constitutive activation. Upon nerve exit in area 1 (Figure 1G), *Chn1*$^{WT/KI}$ *Epha4*$^{KO/KO}$

and *Chn1*$^{KI/KI}$ *Epha4*$^{KO/KO}$ embryos displayed normalized abducens exit and fasciculation (Figure 5, A–E), indicating there is a potential re-balancing of mutant α2-chimaerin signaling upon removal of EphA4 within area 1. By contrast, stalling at area 2 worsened in *Chn1*$^{WT/KI}$ *Epha4*$^{KO/KO}$ compared with *Chn1*$^{WT/KI}$ embryos (Figure 5, A and B), reflected both in reduced abducens nerve length (Figure 5F) and thinner nerve diameter near the orbit (Figure 5G). Moreover, stalled projections in *Chn1*$^{WT/KI}$ *Epha4*$^{KO/KO}$ and *Chn1*$^{KI/KI}$ *Epha4*$^{KO/KO}$ embryos did not stay within normal WT nerve boundaries (Supplemental Video 6), but instead wandered to track with the mandibular and cervical branches of the facial nerve, similar to the *Epha4*$^{KO/KO}$ embryos (Figure 5, I–L). There was a trend toward fewer wandering abducens bundles in *Chn1*$^{WT/KI}$ *Epha4*$^{KO/KO}$ and *Chn1*$^{KI/KI}$ *Epha4*$^{KO/KO}$ compared with *Epha4*$^{KO/KO}$ embryos (Figure 5H), presumably from enhanced nerve stalling. A transverse (top-down) view of abducens whole mount projections revealed wandering abducens projections in more detail (Figure 5, M–P, and Supplemental Figure 3, D–G), demonstrating that the abducens nerve stalling and wandering phenotype in *Chn1*$^{KI/KI}$ *Epha4*$^{KO/KO}$ embryos (Figure 5P and Supplemental Figure 3G) is distinct from, but has features of, *Epha4*$^{KO/KO}$ abducens nerve wandering (Figure 5N and Supplemental Figure 3E) and *Chn1*$^{KI/KI}$ nerve stalling (Figure 5O and Supplemental Figure 3F). Finally, within area 3 at E16.5, *Chn1*$^{KI/KI}$ *Epha4*$^{KO/KO}$ innervation was indistinguishable from *Chn1*$^{KI/KI}$ orbits (Figure 2B): the abducens nerve failed to innervate the lateral rectus, which instead was innervated by aberrant branches of the oculomotor nerve (Figure 5Q). This area 3 phenotype was worse than that of *Epha4*$^{KO/KO}$ embryos. In *Epha4*$^{KO/KO}$ orbits, the lateral rectus muscle was appropriately innervated by the abducens nerve (Figure 5R), although occasionally the nerve appeared thinner than in WT embryos and had minor aberrant innervation of the lateral rectus from the oculomotor nerve (data not shown).

Thus, there appears to be a complex genetic interaction between α2-chimaerin and EphA4 driving the growth of the abducens nerve; in *Chn1*$^{WT/KI}$ *Epha4*$^{KO/KO}$ or *Chn1*$^{KI/KI}$ *Epha4*$^{KO/KO}$ embryos, some features of the abducens phenotype were rescued, some were worsened, and others were unaltered. These data support interactions between mutant α2-chimaerin and EphA4 signaling pathways that alter development of the abducens nerve differently than each individual allele. Additionally, similar to the slight abducens nerve phenotype modification seen in the *Chn1*$^{KO/KO}$ *Epha4*$^{KO/KO}$ cross, these results suggest other pathways could be involved either upstream of mutant α2-chimaerin or downstream of EphA4.

Abducens axons respond to ephrin forward and reverse signaling in explant cultures, and both responses are altered in Chn1$^{KI/KI}$ *explants*. In addition to traditional EphA4 repulsive forward signaling, whereby EphA4 acts as a neuronally expressed receptor to generate axon repulsion, EphA4 can also function as an attractant ligand for ephrin reverse signaling, working in coordination with glial cell–derived neurotrophic factor (GDNF) and its receptors to guide spinal motor neurons. In this system, the coordinated signaling between ephrin-A/Ret and GFRα1/Ret co-receptor pathways upon EphA4+GDNF co-ligand stimulation elicits an outgrowth response beyond that achieved solely by mesenchymal EphA4 signaling through an ephrin-A5/Ret complex or by GDNF signaling through its cognate GFRα1/Ret receptors (32).

The complex genetic interaction between α2-chimaerin and EphA4 in the abducens nerve of our double mutant crosses led us to ask whether abducens neurons use bidirectional EphA4 signaling upstream of α2-chimaerin to guide development. *Epha4* and ephrin-A5 expression at E11.5 supported this possibility: *Epha4* was expressed in the orbital EOM anlage, which was the targeted innervation area of the abducens nerve (Figure 6A), while ephrin-A5 was expressed in E11.5 abducens neurons (Figure 6B and Supplemental Figure 4A), suggesting EphA4 may be used as a ligand to mediate attraction via neuronally expressed ephrin.

In order to test the effects of ephrin forward and reverse signaling on abducens outgrowth, we developed a modified Sholl analysis approach to compare maximum outgrowth (average maximum neurite distance) and total outgrowth (average area under the entire curve) of WT and mutant embryonic abducens explants maintained in culture with recombinant growth factors and/or guidance cues (Supplemental Figure 4, B and C). There were no differences in outgrowth between *Chn1*$^{WT/WT}$ and *Chn1*$^{WT/KI}$ abducens explants cultured without growth factors, demonstrating again that mutant α2-chimaerin is not constitutively hyperactive at baseline (Figure 6, C, D, and K–M).

For ephrin signaling experiments, abducens explants were grown in GDNF because explants grown in ephrin-A5 without growth factor displayed extremely diminished levels of outgrowth (Supplemental Figure 4, D–H). Explants grown in EphA4 alone displayed slightly increased outgrowth, similar to previous reports of spinal motor neurons (32) (Supplemental Figure 4, I–M). *Chn1*$^{WT/WT}$ and *Chn1*$^{WT/KI}$ abducens explant outgrowth did not differ in high concentrations of GDNF (25 ng/ml GDNF+ immunoglobin FC [fragment, crystallizable] domain to control for recombinant FC-fusion proteins) (Figure 6, E, F, N, Q, and R). Thus, the addition of 25 ng/ml GDNF permitted reliable quantification of outgrowth in both forward and reverse ephrin signaling conditions, and permitted testing of the combinatorial effects from EphA4+GDNF stimulation on abducens outgrowth.

Chn1$^{WT/WT}$ explants grown in ephrin-A5+GDNF displayed a significant reduction in maximum outgrowth compared with WT explants grown in FC+GDNF (Figure 6, C, G, N, O, and Q), confirming that abducens explants are repelled by ephrin-A5. *Chn1*$^{WT/KI}$ explants displayed significantly less maximum and total explant outgrowth in ephrin-A5+GDNF than *Chn1*$^{WT/WT}$ explants (Figure 6, G, H, O, Q, and R), supporting the hypothesis that gain-of-function α2-chimaerin mutations increase ephrin-A5–mediated repulsion through canonical ephrin forward signaling. Notably, *Chn1*$^{KO/KO}$ and *Epha4*$^{KO/KO}$ abducens explants had maximum and total outgrowth in ephrin-A5+GDNF similar to that observed in FC+GDNF (Supplemental Figure 4, N–W, and Figure 6, E and N). The lack of responsiveness to ephrin-A5 was similar in the two knockouts, again suggesting that EphA4 is an upstream regulator of α2-chimaerin–mediated repulsive signaling to ephrin-A5 in abducens neurons.

Abducens outgrowth differences were also noted with ephrin reverse signaling. *Chn1*$^{WT/WT}$ abducens explants displayed significantly increased total outgrowth in EphA4+GDNF compared with FC+GDNF (Figure 6, E, I, N, P, and R), indicating that abducens neurons are capable of using ephrin reverse signaling to potentiate axon outgrowth in vitro. Remarkably, *Chn1*$^{WT/KI}$ explants did not have increased outgrowth in the presence of EphA4+GDNF and

instead had outgrowth similar to that in FC+GDNF (Figure 6, E, F, I, J, N, and P–R). These results indicate that mutant α2-chimaerin is recruited downstream of ephrin reverse signaling to attenuate the normal increase in abducens outgrowth that is seen upon addition of EphA4 in WT abducens cultures.

We cultured *Chn1*$^{KO/KO}$ explants to investigate whether α2-chimaerin was necessary for ephrin reverse signaling. We found that when grown in EphA4+GDNF, outgrowth increased to a similar extent in *Chn1*$^{KO/KO}$ and WT explants (Supplemental Figure 4, X–BB). Thus, while WT α2-chimaerin is not necessary for ephrin reverse signaling in abducens motor neurons, mutant α2-chimaerin generates an alternate, gain-of-protein-function that dampens abducens outgrowth in response to ephrin reverse signaling, which may support the recruitment of α2-chimaerin via an indirect feedback loop.

Ret and p75^{NTR} *are candidate co-receptors to mediate ephrin reverse signaling upstream of mutant α2-chimaerin in abducens neurons*. While the involvement of α2-chimaerin in ephrin forward signaling has been previously characterized (12–15, 29), to our knowledge the role of mutant α2-chimaerin in ephrin reverse signaling is novel. Ephrin-A lacks an intracellular signaling domain and requires a co-receptor for reverse signaling. In addition to the Ret/GDNF/GFRα1 spinal motor neuron signaling pathway described above (32), p75^{NTR} has been shown to act as an ephrin-A co-receptor in retinal ganglion cells (RGCs) (33).

The small number of abducens neurons precludes biochemical pathway analysis to directly ascertain whether Ret and/or p75^{NTR} are recruited for ephrin reverse signaling upstream of α2-chimaerin in mutant abducens neurons. Thus, to gain initial insight into these pathways, we harnessed the Sholl analysis method to characterize outgrowth of *Chn1* WT and mutant abducens explants upon stimulation of Ret or p75^{NTR} pathways.

From our EphA4+GDNF abducens Sholl analysis (Figure 6, I, J, and P–R), it appears likely that Ret is used as a co-receptor for ephrin reverse signaling in abducens neurons. To further investigate the contribution of Ret signaling upstream of mutant α2-chimaerin in abducens neurons, we cultured explants in a low concentration of GDNF (1 ng/ml), as previous studies have indicated that the exogenous concentration of GDNF is important for regulating robust GDNF signaling (34). Intriguingly, we found that at low GDNF concentrations there was a significant difference in outgrowth between WT and mutant explants. WT abducens explants trended toward increased outgrowth in low GDNF concentrations compared with conditions without growth factor (FC alone), whereas *Chn1*$^{WT/KI}$ explants showed outgrowth similar to that without growth factor and significantly reduced outgrowth compared with WT (Figure 7, A–E, and Figure 6K). Thus, the lower concentration of GDNF reveals altered activity of mutant α2-chimaerin downstream of GDNF/Ret signaling. Differences between WT and mutant explants were eliminated at higher GDNF concentrations, as both showed significantly increased outgrowth compared with control (Figure 7, D and E, and Figure 6, K and N). Future pathway analyses will elucidate the signaling mechanisms of mutant α2-chimaerin either directly or indirectly downstream of ephrin-A/Ret receptor signaling.

To ascertain whether p75^{NTR}-mediated co-receptor pathways might also activate mutant α2-chimaerin to alter abducens outgrowth in vitro, we added NGF as a p75^{NTR} ligand to WT and *Chn1*$^{WT/KI}$ abducens explants. Interestingly, WT abducens explants grown in NGF (5 ng/ml) showed significantly increased outgrowth compared with conditions without growth factors (Figure 7, F, H, L, and M, and Figure 6, C and K). By contrast, *Chn1*$^{WT/KI}$ abducens explants displayed significantly reduced outgrowth compared with WT controls, instead exhibiting outgrowth similar to that of explants without growth factor (Figure 7, F–H, L, and M, and Figure 6, C, D, and K). Higher concentrations of NGF (25 ng/ml) reduced outgrowth of WT explants to control levels, such that the differences between WT and mutant abducens outgrowth were eliminated (Figure 7, I–M, and Figure 6, C, D, and K). These experiments reveal that both Ret and p75^{NTR} have the potential to be used as ephrin co-receptors in abducens neurons.

Neuronal and mesenchymal Epha4 conditional knockouts reveal abducens phenotypes that differ from each other and from Epha4$^{KO/KO}$. Our in vitro explant data support the hypothesis that the complex genetic interaction between α2-chimaerin and EphA4 in abducens could result, at least in part, from the recruitment of α2-chimaerin in both ephrin forward and reverse signaling. Thus, we conditionally knocked out *Epha4* selectively in motor neurons or in the mesenchyme surrounding the peripheral nerve to evaluate the outgrowth of abducens axons with loss of ephrin forward or reverse signaling, respectively. We selectively removed EphA4-mediated ephrin forward signaling using an *Isl*$^{Cre/+}$ mouse (35), in which Cre is present in *Isl*-expressing cranial and spinal motor neurons and not in the surrounding mesenchyme (Supplemental Figure 5A). To confirm *Isl*^{Cre} activity in abducens neurons, we generated *Chn1*$^{KI/KI}$ *Isl*$^{Cre/+}$ mice, in which *Chn1* is knocked out of motor neurons. Indeed, we detected the anticipated *Chn1*$^{KO/KO}$ abducens phenotype (Supplemental Figure 5B). Next, to determine the effect of removing EphA4-mediated ephrin forward signaling in motor neurons, we analyzed *Epha4*$^{fl/fl}$ *Isl*$^{Cre/+}$ embryos and found that, similar to *Epha4*$^{KO/KO}$ embryos, *Epha4*$^{fl/fl}$ *Isl*$^{Cre/+}$ embryos had a significant increase in the number of wandering bundles compared with controls (Figure 8, A–D and L, and Figure 5H). Compared with *Epha4*$^{KO/KO}$ embryos, however, *Epha4*$^{fl/fl}$ *Isl*$^{Cre/+}$ embryos also displayed a significant increase in the number of abducens nerve bundles following exit from the hindbrain compared with WT *Isl*^{Cre} controls (Figure 8I and Figure 5E), significant reductions in both abducens nerve length and diameter at the orbit (Figure 8, J and K, and Figure 5, F and G), and visibly larger wandering abducens nerve bundles that exhibited enhanced nerve pausing at the midpoint decision within area 2 (Figure 8, A–D, Supplemental Figure 5, H, I, and L, Figure 5N, and Supplemental Video 7). Therefore, selectively removing *Epha4* from motor neurons results in an abducens phenotype distinct from *Epha4*$^{KO/KO}$. These data alone support a role for both EphA4-mediated ephrin forward and reverse signaling in abducens development.

In an analogous approach, to directly investigate the role of EphA4-mediated ephrin reverse signaling in abducens development, we knocked out mesenchymal *Epha4* expression by generating *Epha4*$^{fl/fl}$ *Twist2*$^{Cre/+}$ mice. *Twist2*^{Cre} had broad expression in the E11.5 mesenchyme through which the abducens and other cranial and spinal nerves grow, but was absent from the brain, hindbrain, and spinal cord (36) (Supplemental Figure 5C). *Epha4* expression was greatly reduced in the mesenchymal tissue through which the abducens nerve projects in *Epha4*$^{fl/fl}$ *Twist2*$^{Cre/+}$ embryos, but was

preserved in the abducens nucleus and CNS (Supplemental Figure 5, D–G). The abducens nerve phenotype in *Epha4*$^{fl/fl}$ *Twist2*$^{Cre/+}$ embryos was very severe and distinct from that in the *Epha4*$^{KO/KO}$ and *Epha4*$^{fl/fl}$ *Isl*$^{Cre/+}$ phenotypes. The abducens nerve exited with significantly fewer nerve bundles (Figure 8I and Figure 5E), which initially wandered in the mesenchymal area adjacent to the hindbrain exit before completely stalling in the mesenchyme (Figure 8, E–H, Supplemental Figure 5, J and K, Figure 5N, and Supplemental Video 8). This led to a dramatic reduction in abducens length and complete lack of both abducens innervation near the orbit and aberrant tracking with the facial nerve (Figure 8, J–L, Figure 5, F–H, and Supplemental Figure 5M).

Together, these in vivo data support that EphA4 is used as a receptor and ligand for ephrin forward and reverse signaling to guide abducens nerve development. Moreover, our in vitro data indicate that WT and mutant α2-chimaerin modulate abducens neuron growth downstream of ephrin forward signaling, while mutant (but not WT) α2-chimaerin modulates abducens neuron growth downstream of ephrin reverse signaling. We anticipate that the complex abducens phenotype in *Chn1*$^{WT/KI}$ *Epha4*$^{KO/KO}$ and *Chn1*$^{KI/KI}$ *Epha4*$^{KO/KO}$ embryos arises, at least in part, from recruitment of mutant α2-chimaerin downstream of both ephrin forward and reverse signaling.

Chn1$^{KI/KI}$ *embryonic mice display trochlear nerve abnormalities, which are unaltered by removing EphA4*. Individuals with DRS harboring *CHN1* mutations can also have mild vertical eye movement abnormalities (3, 9). Thus, we investigated whether DRS-mutant *Chn1* in mouse alters oculomotor or trochlear nerve development. Notably, while we found aberrant innervation by the oculomotor nerve of the lateral rectus muscle within the orbit secondary to absence of the abducens nerve (Figure 2, A and B) (24), its trajectory was otherwise indistinguishable from WT (Figure 1, D, E, G, and H, and Supplemental Videos 1 and 2). Thus, our results with endogenous mutant *Chn1* expression differ from the reported oculomotor stalling that follows overexpression of mutant *Chn1* in chick and zebrafish (3, 18, 23). We did, however, find errors in trochlear nerve projection in *Chn1*$^{KI/KI}$ embryos at E11.5, consistent with hypoplasia of its target, the superior oblique muscle, reported in some affected individuals (4, 9).

In E11.5 WT embryos, trochlear axons projected dorsally, crossed the midline in the tectum, exited the brainstem, and fasciculated into a single nerve bundle that projected anteriorly toward the contralateral superior oblique (Figure 9A and Supplemental Video 1). In E11.5 *Chn1*$^{WT/KI}$ and *Chn1*$^{KI/KI}$ embryos, trochlear axons crossed the midline and exited dorsally as in WT embryos, but the axons formed multiple fascicles instead of one nerve bundle, most of which extended appropriately toward the contralateral orbit, but some of which turned back and misprojected toward the ipsilateral orbit (Figure 9B and Supplemental Video 2).

Trochlear nerve projections in *Chn1*$^{KO/KO}$ and *Epha4*$^{KO/KO}$ embryos were unaffected (Figure 9, C and D, and Supplemental Videos 3 and 5), suggesting that WT α2-chimaerin and EphA4 may not be necessary for trochlear nerve guidance, even though mutant α2-chimaerin altered trochlear nerve development. However, trochlear neurons/axons expressed *Chn1*, *Epha4*, and ephrin-A5 (Supplemental Figure 2A and Figure 9, E–G), and ephrin-A5 was expressed in a strong graded pattern in the midbrain tectum near where trochlear nerve projections crossed the dorsal midline (Figure 9H). Thus, expression indicates it is possible for trochlear neurons to use bidirectional ephrin signaling via mutant α2-chimaerin, and we returned to the modified Sholl approach to investigate this possibility.

Chn1$^{WT/WT}$ and *Chn1*$^{WT/KI}$ trochlear explants cultured under control conditions did not have significantly different outgrowth; thus, α2-chimaerin did not appear to be constitutively hyperactive at baseline (Figure 9I and Supplemental Figure 6, A and B). Outgrowth of *Chn1*$^{WT/WT}$ trochlear explants grown in ephrin-A5+GDNF was indistinguishable from outgrowth in FC+GDNF (Figure 9, I, J, and L, and Supplemental Figure 6, A and C). *Chn1*$^{WT/KI}$ explants had a modest, but significant, reduction in outgrowth in ephrin-A5+GDNF compared with WT explants (Figure 9, J and L, and Supplemental Figure 6, C and D). Thus, in the correct circumstances, hyperactive α2-chimaerin can be recruited downstream of ephrin forward signaling to alter trochlear outgrowth. Outgrowth of WT trochlear explants grown in EphA4+GDNF did not significantly differ from that in FC+GDNF (Figure 9, I, K, and L, and Supplemental Figure 6, A and E), and there was no difference in outgrowth between *Chn1*$^{WT/WT}$ and *Chn1*$^{WT/KI}$ explants in EphA4+GDNF (Figure 9, K and L, and Supplemental Figure 6, E and F). These in vitro experiments indicate that trochlear neurons do not predominantly use ephrin forward or reverse signaling, despite expression of *Epha4* and ephrin-A5 in trochlear axons. In vivo, trochlear nerve projections were normal in *Epha4*$^{fl/fl}$ *Isl*$^{Cre/+}$ and *Epha4*$^{fl/fl}$ *Twist2*$^{Cre/+}$ embryos (Figure 9, M and N), further indicating that bidirectional signaling using EphA4 is not critical for trochlear nerve development. Finally, we crossed *Chn1*^{KI} and *Epha4*^{KO} lines to determine whether loss of EphA4 modified the *Chn1*^{KI} trochlear nerve projection abnormalities. *Chn1*$^{KI/KI}$ *Epha4*$^{KO/KO}$ embryos had trochlear abnormalities similar to those of *Chn1*$^{KI/KI}$ embryos (Figure 9, B, O, and P), and thus the *Chn1*^{KI} trochlear phenotype was largely unaltered by the *Epha4*^{KO} allele. Thus, distinct from the use of bidirectional ephrin signaling upstream of α2-chimaerin in abducens neurons, mutant α2-chimaerin likely acts downstream of non-ephrin-mediated pathways to modulate trochlear nerve development.

Chn1$^{KI/KI}$ *embryonic mice display first cervical spinal (C1) nerve abnormalities, which are restored by removing EphA4*. Finally, we examined non-ocular motor neuron populations in E11.5 *Chn1*$^{KI/KI}$ embryos and found a selective defect in the projection of the first cervical spinal (C1) nerve. In *Chn1*$^{WT/WT}$ E11.5 mice, C1 exited the spinal cord ventrally to meet with projections of the hypoglossal nerve (Figure 10A and Supplemental Video 1). In *Chn1*$^{WT/KI}$ and *Chn1*$^{KI/KI}$ embryos, C1 exited the brainstem appropriately, but turned dorsally toward the dermomyotome with variable bilateral penetrance (Figure 10B and Supplemental Video 2).

By contrast to *Chn1*^{KI} embryos, C1 nerve projections were similar to WT controls in *Chn1*$^{KO/KO}$, *Epha4*$^{KO/KO}$, *Epha4*$^{fl/fl}$ *Isl*$^{Cre/+}$, and *Epha4*$^{fl/fl}$ *Twist2*$^{Cre/+}$ embryos (Figure 10, C–F, and Supplemental Figure 7, A and B). Therefore, we asked whether C1 neurons are similar to trochlear neurons and do not rely on WT α2-chimaerin or EphA4 for proper development. C1 neurons/nerve bundles expressed *Chn1*, *Epha4*, and ephrin-A5 (Supplemental Figure 2C and Figure 10, G–J), and *Epha4* was expressed in the mesenchyme through which C1 axons extend and target in E11.5 embryos (Figure 10I), demonstrating proper expression that could support bidirectional ephrin signaling. Thus, we cultured *Chn1* WT and

mutant C1 explants to further examine the contribution of bidirectional ephrin signaling upstream of α2-chimaerin in C1 neurons.

Chn1$^{WT/WT}$ and *Chn1*$^{WT/KI}$ C1 explants have similar outgrowth in FC+GDNF, supporting lack of constitutively hyperactivate *Chn1* in mutant C1 motor neurons (Figure 10, K, N, and O, and Supplemental Figure 7, C and D). Unlike trochlear explants but similar to abducens explants, *Chn1*$^{WT/WT}$ C1 explants exhibited significantly reduced initial outgrowth in ephrin-A5+GDNF compared with FC+GDNF outgrowth (Figure 10, K, L, and N, and Supplemental Figure 7, C and E), demonstrating that WT C1 neurons respond to ephrin forward signaling. *Chn1*$^{WT/KI}$ C1 explants grown in ephrin-A5+GDNF had a significant further reduction in outgrowth compared with WT explants (Figure 10, L, N, and O, and Supplemental Figure 7, E and F), supporting enhanced repulsion of mutant C1 axons to ephrin-A5. By contrast, C1 explant outgrowth in EphA4+GDNF did not differ in WT, mutant, and FC+GDNF conditions (Figure 10, K, M, and O, and Supplemental Figure 7, C, D, G, and H), demonstrating that similar to trochlear explants and distinct from abducens explants, C1 neurons do not use EphA4 as a ligand for ephrin reverse signaling to guide C1 projections in vitro.

Because we found that C1 neurons use repellent ephrin forward signaling and not attractant ephrin reverse signaling upstream of α2-chimaerin in vitro, we asked whether removing *Epha4* would rebalance the activity of mutant α2-chimaerin in *Chn1*$^{KI/KI}$ embryos. Remarkably, *Chn1*$^{WT/KI}$ *Epha4*$^{KO/KO}$ or *Chn1*$^{KI/KI}$ *Epha4*$^{KO/KO}$ embryos had normal C1 projections (Figure 10P), demonstrating that removal of *Epha4* reverses the *Chn1*$^{KI/KI}$ C1 guidance defects and restores normal C1 guidance. These in vitro and in vivo data support that aberrant C1 turning in *Chn1*$^{KI/KI}$ embryos is mediated through ephrin forward signaling and indicate it is possible to restore the normal growth of *Chn1* mutant projections by removing key upstream repellent receptors.

Discussion

Chn1$^{KI/KI}$ *mice reveal abducens guidance defect as a primary etiology of DRS*. Neuronal pathfinding is essential for establishing functional circuits to elicit normal behavior. We report that *CHN1* mutations identified in human patients, when modeled in the mouse, cause primary abducens nerve stalling within the mesenchyme, preventing the abducens nerve from contacting the lateral rectus muscle. Within the orbit, the oculomotor nerve sends stereotypical aberrant branches to misinnervate the lateral rectus, which has recently been shown to also occur secondarily to the absence of abducens motor neurons (24). Together, these studies strongly indicate that DRS results from a primary developmental insult to the abducens nucleus or nerve that prevents its innervation of the lateral rectus. Following this innervation failure, the oculomotor nerve secondarily substitutes innervation to the lateral rectus.

The Duane syndrome phenotype arises during early embryonic development at stages that correspond with approximately 5 weeks human gestation (37), and the early embryonic onset likely precludes practical therapeutic intervention. However, mechanisms that guide opportunistic innervation of the lateral rectus by the oculomotor nerve may provide insights into principles of misinnervation that are involved in other disorders, such as inappropriate facial nerve innervation following injury or surgery. Moreover, the *Chn1*$^{KI/KI}$ mouse provides a tool with which to further investigate cellular and circuit mechanisms underlying DRS and to elucidate general principles of axon guidance that are relevant to human neurodevelopment and neuromuscular innervation.

α2-Chimaerin is critical for proper abducens guidance during embryonic development. We demonstrate that loss and gain of α2-chimaerin function alter abducens nerve guidance, proving that WT α2-chimaerin activity is essential for normal abducens development. Removing or enhancing α2-chimaerin signaling in abducens neurons causes different nerve guidance phenotypes, as well as distinct phenotypes in different populations of motor neurons. *Chn1*$^{KI/KI}$ mice have altered abducens, trochlear, and C1 projections, whereas *Chn1*$^{KO/KO}$ mice display a different abducens nerve guidance phenotype, normal C1 and trochlear projections, but altered gait circuitry and limb innervation (12, 14, 15, 29). Thus, an increase or decrease in α2-chimaerin activity has unique consequences on different neuronal cell types, which may lend insight into its specific functions in different motor neuron populations.

EphA4-mediated ephrin forward and reverse signaling are both critical for proper abducens guidance during embryonic development. Ephrin forward and reverse signaling has been characterized as guiding the axonal projections of limb-innervating motor neurons (32, 38, 39), and α2-chimaerin is known to act downstream of ephrin forward signaling in several neuronal types (12–15), including limb motor neurons (29). We expand on these findings to define the involvement of EphA4-mediated ephrin forward and reverse signaling in abducens nerve development and in a human developmental disorder. We find that selective reduction of ephrin forward signaling by knocking out EphA4 in motor neurons reduces successful lateral rectus targeting of the abducens nerve, perhaps because axons lose the appropriate level of repulsion from incorrect targets. Selectively reducing ephrin reverse signaling by knocking out EphA4 in the mesenchyme causes severe abducens stalling, likely because the nerve is not properly recruited through the mesenchyme toward its target. Both of these abducens phenotypes are more severe than the complete *Epha4*$^{KO/KO}$; therefore, disrupting the balance of attraction or repulsion alone during axon navigation can be more detrimental than interfering with both simultaneously.

α2-Chimaerin and EphA4 exhibit varied genetic interactions in different motor neuron populations. We have identified a complex genetic interaction between *Epha4* and *Chn1*^{KI} in abducens nerve development, which we find can be explained, in part, by the role of mutant α2-chimaerin downstream of both ephrin forward and reverse signaling. Intriguingly, abducens, trochlear, and C1 nerve phenotypes are reversed to varying degrees in *Chn1*$^{KI/KI}$ *Epha4*$^{KO/KO}$ mice, which our in vitro experiments demonstrate can be partially accounted for by the different recruitment of mutant α2-chimaerin in ephrin forward and reverse signaling in these motor neuron subtypes. Our data provide insight into potential mechanisms that generate selective vulnerability of abducens neurons to non-constitutively hyperactivating α2-chimaerin mutations. We propose four nonexclusive scenarios to account for the varying degrees of EphA4/α2-chimaerin genetic interaction in abducens, trochlear, and C1 neurons:

First, *Chn1*$^{KI/KI}$ *Epha4*$^{KO/KO}$ may reverse a *Chn1*$^{KI/KI}$ phenotype to normal WT patterns when EphA isoforms are used only as neuronal receptors for ephrin forward signaling to mediate repulsion,

and not as ligands in ephrin reverse signaling, as supported by our C1 neuronal experiments.

Second, additional non-ephrin signaling pathways likely signal through α2-chimaerin, as indicated by the slight differences in *Chn1*$^{KO/KO}$ and *Epha4*$^{KO/KO}$ abducens nerve phenotypes and by the unaltered trochlear phenotype in *Chn1*$^{KI/KI}$ *Epha4*$^{KO/KO}$ embryos. BDNF/TrkB and semaphorin/plexin/neuropilin signaling pathways have been shown to act upstream of α2-chimaerin in various neuronal types (11, 16, 18); it will be of future interest to determine the contribution of these and other guidance pathways in *Chn1*$^{KI/KI}$ phenotypes.

Third, distinct receptor composition in different neuronal subtypes may mediate integration of different ligands that act through α2-chimaerin to yield different phenotypes. We show that abducens neurons use ephrin reverse signaling upstream of mutant α2-chimaerin in vitro to mediate increased outgrowth. The signaling mechanisms underlying this phenomenon remain an area for further investigation, as it appears that α2-chimaerin may not normally act downstream of ephrin reverse signaling, but rather is recruited under gain-of-function mutant conditions. Similar to reports in limb motor neurons (32), ephrin-A5 could use Ret as a co-receptor for reverse signaling in concert with GFRα1/Ret signaling to mediate potentiated outgrowth of abducens neurons in response to EphA4 and GDNF ligands. In this case, DRS-mutant α2-chimaerin may misregulate signaling pathways downstream of Ret to dampen increased outgrowth. Alternatively, if abducens neurons use p75^{NTR} as a co-receptor for ephrin reverse signaling similar to RGCs (33), mutant α2-chimaerin may act downstream of p75^{NTR} to enhance axon repulsion. Ret and p75^{NTR} co-receptor pathways could be recruited simultaneously in abducens neurons to modulate ephrin reverse signaling, thus combining elements of RGC and limb motor neuron axon guidance and accounting for an additional layer of phenotype specificity and complexity.

Last, expression of different cytoskeletal regulatory pathways (i.e., RacGAPs/GEFs) in specific motor neuron populations may modulate the signaling contribution of α2-chimaerin. The varied expression and recruitment of diverse RacGAP/GEF pathways in different motor neuron populations may further influence phenotype rescue and selective vulnerability.

Further investigation into the mechanisms underlying the selective ephrin- and non-ephrin-mediated signaling pathways upstream of α2-chimaerin may lead to the identification of additional genetic contributions to DRS.

Mutant α2-chimaerin informs the complexity of axon guidance signaling pathways in neuronal development. Our data highlight the importance of investigating molecular mechanisms in a cell type–specific manner. Despite the technical challenges posed by the limited number of abducens motor neurons that project to a discrete muscle target (40), we are able to combine in vivo genetic interaction studies and motor neuron subtype–specific in vitro cultures to assess the implications of altered signaling pathways on abducens development. We find that even this simple neuronal circuit uses intricate guidance pathways to establish connectivity, which can serve as a model from which to investigate the breadth of signaling complexity that exists between various guidance receptors during development. By using a gain-of-function DRS-causing mutation in *CHN1*, we identify the importance of signaling balance in neuronal circuit formation. In our experimental paradigm, α2-chimaerin loss of function does not appear to perturb ocular motor circuit formation nearly as much as altered function, highlighting the sensitivity of neuronal guidance mechanisms and the importance of investigating physiologic gain-of-function mutations in neurological disorders. Thus, our investigation into the effects of hyperactivated α2-chimaerin on motor neuron development not only provides insight into DRS etiology and selective vulnerability, but also informs broad principles that guide neuronal circuit formation.

Methods

Chn1^{KI} *mouse construct*. InGenious Targeting Laboratory Inc. created the *Chn1*^{KI} targeting vector to introduce an 60A>T missense change in exon 3 of *Chn1* and inserted it into a mouse 129 (RP22:77N16) BAC clone. The mutation-containing BAC construct was confirmed by restriction analysis and sequencing and injected into mouse embryonic stem (ES) cells by the Boston Children's Hospital Intellectual and Developmental Disabilities Research Center (IDDRC) Mouse Gene Manipulation Core. Targeted ES cells were screened using PCR, Southern blot analysis, and sequencing for proper insertion and correct sequence. Knockin mice were confirmed by genotyping.

Generation of Chn1$^{KO/KO}$ *mice*. *Chn1*$^{KI/KI}$ mice were crossed with *E2a-Cre* and *Prm-Cre* transgenic mice to create germline-knockout *Chn1*$^{KO/KO}$ mice. Removing *Chn1* exon 3 preserves promoter and regulatory elements required for α1-chimerin expression (41).

Additional mouse strains. Littermate controls were used whenever possible; controls from the same genetic background were always used for any given experiment. See Supplemental Table 1 for detailed strain information.

Antibodies. The following antibodies were used: mouse anti-neurofilament (Developmental Studies Hybridoma Bank [DSHB], 2H3 ascites fluid), rabbit anti-GFP (Invitrogen, a11122), rabbit anti-CHN1 (Abcam, EPR9906), rabbit anti-GAPDH (Santa Cruz Biotechnology Inc., sc-25778), rabbit anti–ephrin-A5 (R&D Systems, AF3743-SP), anti-actin α-smooth muscle–Cy3 antibody (Sigma-Aldrich, C6198), mouse anti-Isl1 concentrate (DSHB, 39.4D5), chicken anti-GFP (Abcam, ab13970), DAPI (Invitrogen, D1306), goat anti-mouse Alexa Fluor 546 (Invitrogen, A-11030), goat anti-rabbit Alexa Fluor 488 or 647 (Invitrogen, A-21311 or A21244), Peroxidase AffiniPure donkey anti-rabbit and donkey anti-mouse IgG (Jackson ImmunoResearch Laboratories Inc., 715-035-151), goat anti-chicken FITC (Abcam, ab46969).

Whole mount embryo staining. E11.5 embryos were fixed in 4% PFA and prepared as previously described (42). Whole embryos were stained with primary 1:500 mouse anti-neurofilament (DSHB) and 1:500 rabbit anti-GFP (Invitrogen); secondary 1:1,000 goat anti-mouse Alexa Fluor 546 (Invitrogen) and 1:1,000 goat anti-rabbit Alexa Fluor 488 or 647 (Invitrogen). Embryos were cleared with 1 part benzyl alcohol:2 parts benzyl benzoate (Sigma-Aldrich) and imaged using a Zeiss LSM710 confocal microscope. Images were processed in 3D using Imaris (Bitplane) to identify similar *z*-planes between embryos. See Supplemental Methods for measurement parameters (27).

Orbital dissections. E16.5 *Isl*^{MN}-GFP–positive mouse embryos from the indicated genetic crosses were prepared as previously described (24).

Chn1$^{KI/KI}$ *Bax*$^{-/-}$ *immunohistochemistry*. E10.5 and E13.5 *Chn1*$^{KI/KI}$ *Bax*$^{-/-}$*Hb9*-GFP embryos were immunostained for ISL1 as previously

described (27). Counts represent bilateral number of motor neurons. Experiments were performed in a blinded manner.

ISH. Digoxigenin-labeled (DIG-labeled) mRNA antisense probes to α2-chimaerin–specific *Chn1*, *Epha4*, ephrin-A5, and *eGFP* were generated as specified in Supplemental Methods. ISH on 20-μm sections was performed by the RNA In Situ Hybridization Core at Baylor College of Medicine using an automated robotic platform as previously described (43), with modifications for double ISH.

Alkaline phosphatase binding assay. The ephrin-A5–AP expression construct was shared by John G. Flanagan (Harvard Medical School, Boston, MA, USA). HEK293-T cells were transfected with the expression construct, then lysate was applied to open-book hindbrain samples as previously described (44).

Recombinant proteins. Recombinant proteins included: GDNF, BDNF, CNTF (ProSpec); mouse EphA4, mouse ephrin-B1, mouse ephrin-B2, human ephrin-A5 (R&D Systems), human IgG FC fragment (EMD Millipore). FC, ephrin-A5, and EphA4 were pre-clustered 1:5 (concentration ratio) with goat anti-human IgG, Fcγ fragment–specific Cy3 (Jackson ImmunoResearch Laboratories Inc.) for 30 minutes at room temperature.

Rac-GTP ELISA. Cortical neuronal cultures were generated as described in Supplemental Methods. Experiments were conducted simultaneously with WT and mutant littermates. Cells were serum starved in DMEM/penicillin/streptomycin for 2 hours, then DMEM or 10 μM PMA in DMEM was added (DMEM: 30 minutes, PMA: 15 or 30 minutes). Cells were washed once with cold PBS, then lysed in ice-cold RIPA. Samples were processed for Rac-GTP levels using a Rac1 G-LISA Activation (Colorimetric Based) Assay Kit (Cytoskeleton Inc.). When possible, 2 replicates per condition were run on the same plate, and O.D. output values were averaged. Averaged values were normalized to O.D. from WT DMEM within each experiment.

Abducens, trochlear, and C1 explant culture. Coverslips were coated with 20 μg/ml poly-D-lysine (Millipore), 10 μg/ml laminin (Invitrogen). GFP^+ embryos were harvested in ice-cold PBS and microdissected in ice-cold HBSS. Microdissection techniques are outlined in Supplemental Methods. Both nuclei were placed into PDL/laminin-coated wells with HBSS on ice during dissection of the remaining littermates. For each well, the 2 explants were positioned at opposite sides of the coverslip, and HBSS was removed and quickly replaced with Neurobasal (Invitrogen), B27 (Invitrogen), 2 mM L-glutamine (Invitrogen), 100 μg/ml penicillin/streptomycin (Invitrogen) containing indicated growth factors and/or proteins.

Growth cone collapse experiments. Abducens explants were grown in 25 ng/ml GDNF, 25 ng/ml BDNF, and 25 ng/ml CNTF for 12–14 hours; transferred to a Nikon Perfect Focus Eclipse Ti live cell fluorescence microscope; and maintained at 37°C with 5% CO_2/95% air. 100 μl of media was removed, recombinant proteins were added, and the mixture was applied. Explants were reimaged once a minute for 30 minutes to assess growth cone dynamics. Measurement parameters are outlined in Supplemental Methods.

Sholl analysis. Abducens, trochlear, and C1 explants were grown in the proteins noted for 18 hours, then fixed with 4% PFA/4% sucrose/PBS. Background fluorescence was subtracted uniformly, and a standard threshold was applied to images. Explant body was outlined manually in Fiji, concentric circles were drawn using a macro at 20-μm intervals, and intersecting axons were counted. WT controls were present in each replicate within every condition, and different protein combinations were compared within at least one experiment per group. Individual samples were graphed, then averaged across experiments within each condition to obtain final outgrowth curves. Outgrowth calculations are discussed in Supplemental Methods.

Statistics. All data were analyzed and graphed using SPSS software (IBM). Statistical methods are provided in each figure legend and include one way ANOVA with Tukey's or Dunnett's test and unpaired two tailed *t* test. $P < 0.05$ was considered statistically significant, except where indicated based on Bonferroni correction. Graphs represent mean ± SEM.

Study approval. All animal work was performed in compliance with protocols approved by the Boston Children's Hospital Institutional Animal Care and Use Committee.

Author contributions

AAN and ECE designed experiments and wrote the manuscript; AAN, JGP, YW, APT, NMG, MMD, and LC conducted experiments and acquired data; AAN and YW analyzed data; WMC established necessary reagents.

Acknowledgments

We thank L. Ding and D. Tom for assistance with Sholl analysis (Harvard NeuroDiscovery Center Enhanced Neuroimaging Core); M. Thompson for ES cell injection (Gene Manipulation Core, BCH IDDRC, NIH P30HD018655); the Dana-Farber/Harvard Cancer Center Rodent Histopathology Core for paraffin embedding (NCI Cancer Center Support Grant NIH P30CA006516); the RNA In Situ Hybridization Core at Baylor College of Medicine and the expert assistance of Cecilia Ljungberg (NIH 1S10OD016167; IDDRC grant NIH U54HD083092, Eunice Kennedy Shriver National Institute of Child Health and Human Development); M.C. Whitman, Y. Su, and H. Marudzinski for technical assistance (Engle laboratory); S.L. Pfaff (Salk Institute for Biological Studies, La Jolla, California, USA) for Isl^{MN}-GFP mice; and Engle laboratory members, J.W. Lichtman, T.L. Schwarz, D. Van Vactor, M. Sahin, and M.A. Tischfield for helpful discussions. AAN was funded by NIH T32AG000222 and ECE is a Howard Hughes Medical Institute Investigator.

Address correspondence to: Elizabeth C. Engle, Boston Children's Hospital, Neurology Research, CLS14075 (BCH3149), 300 Longwood Ave, Boston, Massachusetts 02115, USA. Phone: 617.919.4030; E-mail: elizabeth.engle@childrens.harvard.edu.

AAN's present address is: Denali Therapeutics, San Francisco, California, USA.

YW's present address is: Xinhua Hospital and Shanghai Jiao Tong University School of Medicine, Shanghai, China.

1. Engle EC. Human genetic disorders of axon guidance. *Cold Spring Harb Perspect Biol*. 2010;2(3):a001784.
2. Nugent AA, Kolpak AL, Engle EC. Human disorders of axon guidance. *Curr Opin Neurobiol*. 2012;22(5):837–843.
3. Miyake N, et al. Human CHN1 mutations hyperactivate alpha2-chimaerin and cause Duane's retraction syndrome. *Science*. 2008;321(5890):839–843.
4. Demer JL, Clark RA, Lim KH, Engle EC. Magnetic resonance imaging evidence for widespread

orbital dysinnervation in dominant Duane's retraction syndrome linked to the DURS2 locus. *Invest Ophthalmol Vis Sci*. 2007;48(1):194–202.
5. Hotchkiss MG, Miller NR, Clark AW, Green WR. Bilateral Duane's retraction syndrome. A clinical-pathologic case report. *Arch Ophthalmol*. 1980;98(5):870–874.
6. Miller NR, Kiel SM, Green WR, Clark AW. Unilateral Duane's retraction syndrome (type 1). *Arch Ophthalmol*. 1982;100(9):1468–1472.
7. Huber A. Electrophysiology of the retraction syndromes. *Br J Ophthalmol*. 1974;58(3):293–300.
8. Chan WM, Miyake N, Zhu-Tam L, Andrews C, Engle EC. Two novel CHN1 mutations in 2 families with Duane retraction syndrome. *Arch Ophthalmol*. 2011;129(5):649–652.
9. Miyake N, et al. Expansion of the CHN1 strabismus phenotype. *Invest Ophthalmol Vis Sci*. 2011;52(9):6321–6328.
10. Hall C, et al. alpha2-chimaerin, a Cdc42/Rac1 regulator, is selectively expressed in the rat embryonic nervous system and is involved in neuritogenesis in N1E-115 neuroblastoma cells. *J Neurosci*. 2001;21(14):5191–5202.
11. Ip JP, et al. α2-chimaerin controls neuronal migration and functioning of the cerebral cortex through CRMP-2. *Nat Neurosci*. 2011;15(1):39–47.
12. Iwasato T, et al. Rac-GAP alpha-chimerin regulates motor-circuit formation as a key mediator of EphrinB3/EphA4 forward signaling. *Cell*. 2007;130(4):742–753.
13. Shi L, et al. Alpha2-chimaerin interacts with EphA4 and regulates EphA4-dependent growth cone collapse. *Proc Natl Acad Sci USA*. 2007;104(41):16347–16352.
14. Wegmeyer H, et al. EphA4-dependent axon guidance is mediated by the RacGAP alpha2-chimaerin. *Neuron*. 2007;55(5):756–767.
15. Beg AA, Sommer JE, Martin JH, Scheiffele P. alpha2-Chimaerin is an essential EphA4 effector in the assembly of neuronal locomotor circuits. *Neuron*. 2007;55(5):768–778.
16. Brown M, et al. Alpha2-chimaerin, cyclin-dependent Kinase 5/p35, and its target collapsin response mediator protein-2 are essential components in semaphorin 3A-induced growth-cone collapse. *J Neurosci*. 2004;24(41):8994–9004.
17. Colón-González F, Leskow FC, Kazanietz MG. Identification of an autoinhibitory mechanism that restricts C1 domain-mediated activation of the Rac-GAP alpha2-chimaerin. *J Biol Chem*. 2008;283(50):35247–35257.
18. Ferrario JE, et al. Axon guidance in the developing ocular motor system and Duane retraction syndrome depends on Semaphorin signaling via alpha2-chimaerin. *Proc Natl Acad Sci USA*. 2012;109(36):14669–14674.
19. Asante CO, et al. Cortical control of adaptive locomotion in wild-type mice and mutant mice lacking the ephrin-Eph effector protein alpha2-chimaerin. *J Neurophysiol*. 2010;104(6):3189–3202.
20. Dottori M, et al. EphA4 (Sek1) receptor tyrosine kinase is required for the development of the corticospinal tract. *Proc Natl Acad Sci USA*. 1998;95(22):13248–13253.
21. Kullander K, et al. Role of EphA4 and EphrinB3 in local neuronal circuits that control walking. *Science*. 2003;299(5614):1889–1892.
22. Serradj N, et al. EphA4-mediated ipsilateral corticospinal tract misprojections are necessary for bilateral voluntary movements but not bilateral stereotypic locomotion. *J Neurosci*. 2014;34(15):5211–5221.
23. Clark C, Austen O, Poparic I, Guthrie S. α2-Chimaerin regulates a key axon guidance transition during development of the oculomotor projection. *J Neurosci*. 2013;33(42):16540–16551.
24. Park JG, et al. Loss of MAFB Function in humans and mice causes duane syndrome, aberrant extraocular muscle innervation, and inner-ear defects. *Am J Hum Genet*. 2016;98(6):1220–1227.
25. Chung M, Stout JT, Borchert MS. Clinical diversity of hereditary Duane's retraction syndrome. *Ophthalmology*. 2000;107(3):500–503.
26. Wichterle H, Lieberam I, Porter JA, Jessell TM. Directed differentiation of embryonic stem cells into motor neurons. *Cell*. 2002;110(3):385–397.
27. Cheng L, et al. Human CFEOM1 mutations attenuate KIF21A autoinhibition and cause oculomotor axon stalling. *Neuron*. 2014;82(2):334–349.
28. Lewcock JW, Genoud N, Lettieri K, Pfaff SL. The ubiquitin ligase Phr1 regulates axon outgrowth through modulation of microtubule dynamics. *Neuron*. 2007;56(4):604–620.
29. Kao TJ, Nicholl GC, Johansen JA, Kania A, Beg AA. α2-chimaerin is required for Eph receptor-class-specific spinal motor axon guidance and coordinate activation of antagonistic muscles. *J Neurosci*. 2015;35(6):2344–2357.
30. Herrmann JE, Pence MA, Shapera EA, Shah RR, Geoffroy CG, Zheng B. Generation of an EphA4 conditional allele in mice. *Genesis*. 2010;48(2):101–105.
31. Lakso M, et al. Efficient in vivo manipulation of mouse genomic sequences at the zygote stage. *Proc Natl Acad Sci USA*. 1996;93(12):5860–5865.
32. Bonanomi D, et al. Ret is a multifunctional coreceptor that integrates diffusible- and contact-axon guidance signals. *Cell*. 2012;148(3):568–582.
33. Lim YS, McLaughlin T, Sung TC, Santiago A, Lee KF, O'Leary DD. p75(NTR) mediates ephrin-A reverse signaling required for axon repulsion and mapping. *Neuron*. 2008;59(5):746–758.
34. Cik M, et al. Binding of GDNF and neurturin to human GDNF family receptor alpha 1 and 2. Influence of cRET and cooperative interactions. *J Biol Chem*. 2000;275(36):27505–27512.
35. Yang L, et al. Isl1Cre reveals a common Bmp pathway in heart and limb development. *Development*. 2006;133(8):1575–1585.
36. Yu K, et al. Conditional inactivation of FGF receptor 2 reveals an essential role for FGF signaling in the regulation of osteoblast function and bone growth. *Development*. 2003;130(13):3063–3074.
37. Otis EM, Brent R. Equivalent ages in mouse and human embryos. *Anat Rec*. 1954;120(1):33–63.
38. Dudanova I, Kao TJ, Herrmann JE, Zheng B, Kania A, Klein R. Genetic evidence for a contribution of EphA:ephrinA reverse signaling to motor axon guidance. *J Neurosci*. 2012;32(15):5209–5215.
39. Marquardt T, et al. Coexpressed EphA receptors and ephrin-A ligands mediate opposing actions on growth cone navigation from distinct membrane domains. *Cell*. 2005;121(1):127–139.
40. Sturrock RR. Stability of neuron and glial number in the abducens nerve nucleus of the ageing mouse brain. *J Anat*. 1989;166:97–101.
41. Dong JM, Smith P, Hall C, Lim L. Promoter region of the transcriptional unit for human alpha 1-chimaerin, a neuron-specific GTPase-activating protein for p21rac. *Eur J Biochem*. 1995;227(3):636–646.
42. Huber AB, et al. Distinct roles for secreted semaphorin signaling in spinal motor axon guidance. *Neuron*. 2005;48(6):949–964.
43. Yaylaoglu MB, Titmus A, Visel A, Alvarez-Bolado G, Thaller C, Eichele G. Comprehensive expression atlas of fibroblast growth factors and their receptors generated by a novel robotic in situ hybridization platform. *Dev Dyn*. 2005;234(2):371–386.
44. Feldheim DA, et al. Topographic guidance labels in a sensory projection to the forebrain. *Neuron*. 1998;21(6):1303–1313.